ISSN 0965-545X, Polymer Science, Ser. A, 2015, Vol. 57, No. 5, pp. 515–551. © Pleiades Publishing, Ltd., 2015.
Original Russian Text © A.L. Volynskii, A.Yu. Yarysheva, E.G. Rukhlya, L.M. Yarysheva, N.F. Bakeev, 2015, published in Vysokomolekulyarnye Soedineniya. Ser. A, 2015, Vol. 57, No. 5, pp. 398–436.

Effect of Spatial Restrictions at the Nanometer Scale on Structuring in Glassy and Crystalline Polymers

A. L. Volynskii[a,*], A. Yu. Yarysheva[a], E. G. Rukhlya[a], L. M. Yarysheva[a], and N. F. Bakeev[a,b]

[a] *Faculty of Chemistry, Moscow State University, Moscow, 119991 Russia*

[b] *Enikolopov Institute of Synthetic Polymer Materials, Russian Academy of Sciences, Profsoyuznaya ul. 70, Moscow, 117393 Russia*

**e-mail: volynskii@mail.ru*

Received November 27, 2014
Revised Manuscript Received March 19, 2015

Abstract—The literature data on the effect of nanometer-scale spatial restrictions on the phase transitions and crystallizability of polymers are analyzed. It is shown that, as the volume of the polymer phase is decreased and its linear sizes take values on the order of 50 nm or less, the fundamental properties of the polymers change abruptly. The glass-transition temperature may decrease by tens of degrees, the temperature and heat of crystallization and the temperature and heat of melting may decline sharply, and the degree of crystallinity of polymers may become lower. Shredding of the polymer into nanometer sizes strongly affects the type of nucleation during its crystallization. As the length of the polymer phase is decreased, the transition from heterogeneous nucleation, which is usually observed during crystallization of bulky polymers, to homogeneous nucleation occurs through the stage of fractional crystallization. The crystallization of polymers under confined conditions is accompanied by the orientation of crystallites in the nanometer asymmetric space and is controlled by the size and morphology of restriction, the character of its interaction with the solid surface, and the ratio of the rates of nucleation and growth of crystals. The analyzed data are of great importance in the manufacture of such miniature objects as nanorods and nanowires necessary for the development and creation of modern devices used to solve important applied problems in microelectronics and biomedicine. The mentioned spatial effects should be taken into account during the creation of nanostructured films for solar cells and polymer membranes of energy separators, for the targeted delivery of drugs, and in many other fields.

DOI: 10.1134/S0965545X15050168

INTRODUCTION

At present, the study of fundamental properties of a substance ground to nanometer sizes is developing vigorously. The properties of solids during their dispersion into nanometer sizes change so substantially and diversely that a large quantity of review papers concerning this problem have been published [1–6].

The influence of nanometer-scale spatial restrictions on the structures and properties of low-molecular-mass solids has been well known for a long time. As an example, the study of thermodynamic properties of the very widely used solvent benzene may be mentioned [7]. Benzene was introduced into nanoporous glasses, and its melting processes were investigated via DSC [8]. Figure 1 presents the typical results of this study.

Without going into details of the mechanism of the observed phenomena, note, first, that melting temperature T_m of benzene decreases during its penetration into narrow (nanosized) pores and, second, the value of depression depends on the diameters of pores: the smaller the diameters of pores, the lower the melting temperature of benzene. Moreover, as follows from Fig. 1, the interval of melting likewise depends on the diameters of pores in the porous glass: the smaller the diameters of pores, the wider the interval of benzene melting. In the narrowest pores, it exceeds 20°C, whereas in the bulk, the interval of benzene melting is not above 5–7°C.

As the diameters of pores decrease, such an important characteristic of a substance as the heat of melting changes as well. As is clear from Fig. 2, beginning from pore diameters of ~25–30 nm, the heat of melting rapidly decreases with decreases in diameters of pores and this reduction may be very pronounced, for example, several-fold [7]. It should be emphasized that the decreases in the temperature and heat of melting in nanopores are of a general pattern and are observed for many low-molecular-mass crystallizable liquids [9].

The effect of nanometer-scale spatial restrictions is likewise distinct in the case of high-molecular-mass compounds (e.g., [10–15]). This circumstance in turn is of great importance for the obtainment of such miniature objects as nanorods and nanofibers and for the development of modern devices used to solve important applied problems in microelectronics, biomedi-

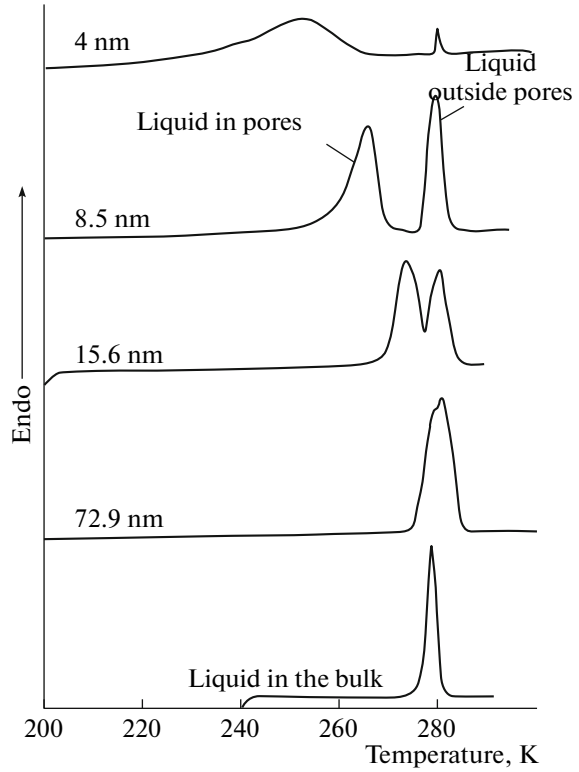

Fig. 1. DSC thermograms of benzene melting in the bulk (the lower curve) and in porous glasses with pore sizes shown on the thermograms [7].

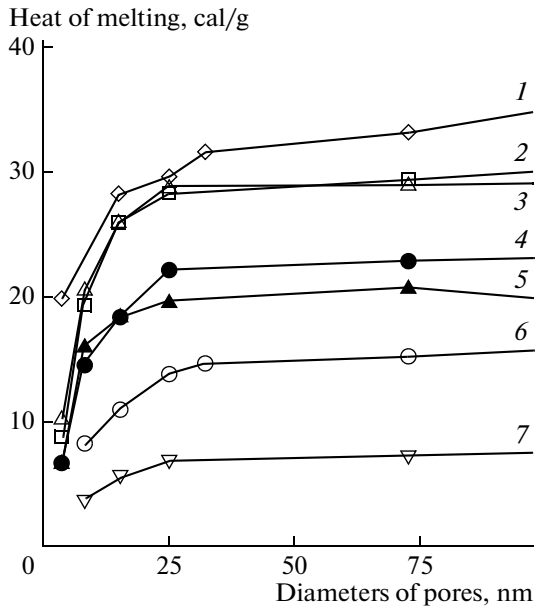

Fig. 2. Heats of melting of organic liquids vs. diameters of pores that they fill for (*1*) naphthaline, (*2*) heptane, (*3*) benzene, (*4*) *trans*-decalin, (*5*) chlorobenzene, (*6*) *cis*-decalin, and (*7*) cyclohexane [7].

cine, and many other areas [16–21]. Considerable progress has been achieved in research into the effect of nanometer-scale spatial restrictions on the structure and properties of amorphous polymers [22].

The present review is devoted to the generalization and analysis of the experimental data demonstrating the effect of geometric spatial restrictions on the structures and properties of polymers. There are several techniques that make it possible to investigate the effect of nanometer-scale spatial restrictions on the structures and properties of polymers. First, there are one-dimensional restrictions implemented in thin films or layers, when the growth of crystals is confined only in one direction (perpendicular to the thickness of a film or layer). In all other directions, the growth of polymer crystals occurs freely, without any restrictions.

Second, there are two-dimensional restrictions. An example of spatial two-dimensional restrictions is the crystallization of polymers in nanoporous cylindrical templates, such as nuclear filters (track membranes) or aluminum oxide plates (AOPs). In these porous media, crystallization is confined in the cylindrical space of a pore.

Finally, there are three-dimensional restrictions, which are implemented in nanosized spherical particles or particles with similar geometries existing in suspensions and emulsions [23]. In this case, the front of the crystallization of the polymer is confined in all directions and these restrictions are the most efficient. In this review, effects of all the above-mentioned kinds of spatial restrictions on the crystallization of polymers will be considered sequentially.

PROPERTIES OF AMORPHOUS POLYMERS IN THIN (NANOMETER) LAYERS

In recent years (beginning in the mid-1990s), major discoveries were made in the field of thin (nanometer) layers of amorphous polymers. The phenomenon of the strongest depression of glass-transition temperatures T_g of amorphous polymers in their thin films and surface layers should be noted above all. The case in point is polymer layers with thicknesses up to tens of nanometers. Nowadays, the general character of this phenomenon is beyond question; however, it was overlooked earlier: in the study of the properties of bulky polymers, the contribution of surface layers to properties was negligibly small and was disregarded. Nevertheless, in cases when a high-level interfacial surface develops during deformation, this contribution should be taken into account. Let us consider the main features of this phenomenon.

Glass-Transition Temperatures of Free-Standing Polymer Films of Nanometer Thicknesses

Methods that make it possible to prepare thin (hundreds of angstroms) films without any substrates,

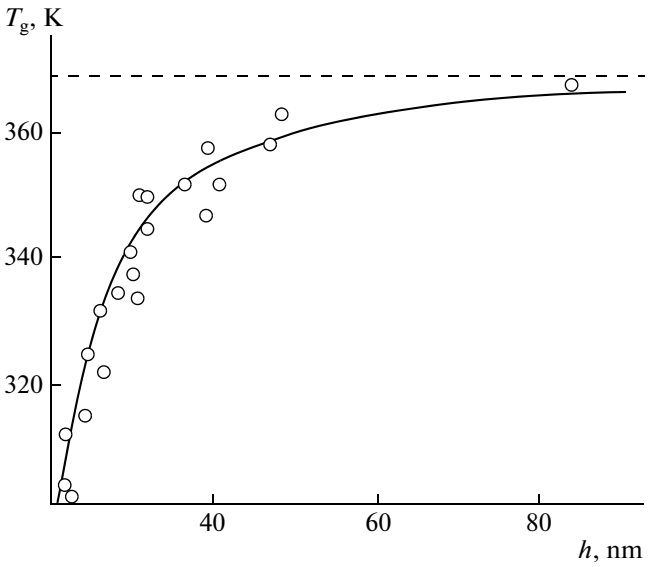

Fig. 3. Plots of T_g of free-standing PS films vs. their thicknesses $M = (116–347) \times 10^3$. The dotted curve is the glass-transition temperature of bulky PS [25].

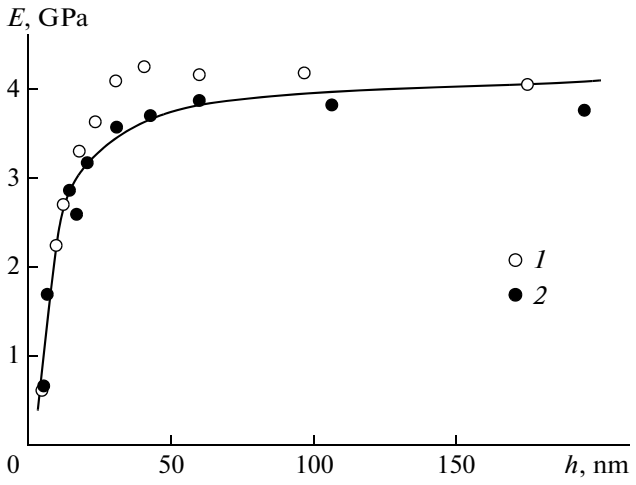

Fig. 4. Young's modulus vs. thickness of the PS film: (*1*) $M_w = 18.0 \times 10^5$ and (*2*) 11.4×10^4 [31].

as well as techniques to measure their T_g values [24], were developed. These films may be prepared two ways. First, the film formed on the substrate is floated on the surface of water and then is picked up on a supporting grid. Second, the films are prepared via evaporation of a thin layer of a polymer solution deposited on the surface of a denser liquid: as a rule, water. In fact, this is the technique for the preparation of supporting film substrates for transmission electron microscopy. After the film is formed on the surface of water, it is placed in a special holder and its properties are investigated.

Because the majority of studies of free-standing films were performed with the use of PS, the experimental data reported by various researchers may be generalized in a common figure [25].

As is clear from Fig. 3, such an important characteristic of a polymer as T_g begins to decrease abruptly when the thickness of the polymer film becomes less than 70–80 nm. The values of T_g depression may attain many tens and even hundreds of degrees. The mechanism of the observed phenomenon is still not clear to the full extent, although reasonable assumptions about this issue were highlighted in detail in the literature [26, 27].

In conclusion of this section, it should be emphasized that a sharp depression of T_g in the surface layers and thin films of glassy polymers is directly confirmed by elastic moduli measurements. In [28–33], the elastic moduli were estimated on the basis of analysis of microreliefs appearing during deformation of bilayer polymer systems. The results of these measurements for glassy PS are presented in Fig. 4 as the dependence of elastic modulus on thickness of the film. It is seen that once the thickness of the PS film becomes less than 50–70 nm, the elastic modulus decreases abruptly, regardless of the molecular mass of the polymer. This decrease attains high values. (The modulus decreases by a factor of 4–5 at most.) These data are consistent with the above-described results of T_g measurements in thin films of glassy polymers (compare Figs. 3 and 4). Hence, the first circumstance that is worth noting is that T_g of the polymer in nanometer layers declines strongly.

Glass-Transition Temperatures of Polymer Films of Nanometer Thicknesses on Solid Substrates

Another important circumstance that should be considered within the context of this review is that the molecular mobility of the polymer with T_g being a measure of this phenomenon depends on the contact of the thin polymer film with various types of interfacial surfaces. Therefore, it is vital to examine in detail how the type and structure of the given boundary affect the glass transitions of polymers.

The depression of T_g of the polymer in thin (nanometer) films deposited on a silicon wafer passivated with hydrogen was first observed via ellipsometry [34]. The film thickness was varied from 300 to 10 nm. It was shown that, starting from a thickness of 40 nm, the glass-transition temperature of PS begins to decline abruptly relative to its value for the bulky polymer. At a film thickness of 10 nm, the depression was 25 K. This value was far beyond the error of glass-transition temperature determination via ellipsometry.

As was shown in [35, 36], the values of T_g frequently decrease appreciably in nanometer-thick films deposited on solid substrates, as in the case of free-standing films considered above. However, in

some cases, the depression of T_g is less distinct [26] or absent or T_g increases significantly [37–40].

For substrate-deposited thin films, the intensity of molecular motion is noticeably affected by the type of interfacial contact [41]. This phenomenon was intelligibly observed, for example, in [42]. The authors of [42] measured electron density in the surface layers of PS, PMMA, and poly(4-vinylpyridine) (PVP) thin films deposited on a SiO_2 substrate with the use of X-ray reflection spectroscopy. The thicknesses of the films were approximately $4R_g$, where R_g is the radius of gyration of a macromolecule. It was found that, for PS and PMMA, electron density near the free surface of the film decreases, while for PVP, this property increases. In accordance with [42], the observed effect is associated with different intensities of interaction between hydrophobic (PS and PMMA) and hydrophilic (PVP) polymers with the polar substrate.

The authors of [43] reported that the type of substrate shows a considerable effect on molecular mobility of the polymer in the substrate-adjoining thin layer. The diffusion coefficients of fluorescently labeled PS macromolecules deposited on quartz substrates were measured with the use of the fluorescence technique [43]. It was shown that, at a film thickness less than 150 nm, the diffusion coefficient decreases. As in [44], the decrease in the diffusion coefficient was explained by a strong interaction with the substrate restricting the molecular mobility of chains.

A similar conclusion was made in [26] on the basis of Brillouin light-scattering and ellipsometry measurements of T_g values in thin PS films as a function of their thicknesses. The data obtained for free-standing films and silica substrate-supported films having different molecular masses were compared. For free-standing films, a sharp (by more than 60°C) depression of T_g was observed for films with thicknesses $h \leq R_{ee}$, where R_{ee} is the unperturbed coil size. For supported films, the depression of T_g was likewise observed, but the magnitude of this depression was as low as 4°C. A marked influence of the substrate on the thermal-expansion coefficient in thin films of deuterated PS was revealed via the method of neutron scattering [45]. It was found that, for deuterated PS, there is a noticeable gradient of the thermal-expansion coefficient over the film thickness, which in turn depends on the type of interfacial contact. This phenomenon was explained by the interaction of the polymer with the substrate.

Birefringence-relaxation studies made it possible to estimate T_g values for ultrathin PS films on glass substrates [35]. As the thickness of the film was decreased from 10 μm to 5.8 nm, the depression of T_g was 15–20°C. In thick films (10 μm), molecules close to the polymer/air interface relax at a higher rate than molecules in contact with the substrate. Considerable restrictions imposed on the molecular mobility in thin PS films on silicon wafer were additionally described in [46], although the thicknesses of the films were much greater than the gyration radius of the molecule. It may be stated that the above restrictiîns of molecular mobility appear because of a strong interaction with the substrate. The electron-density gradient in the direction perpendicular to the plane of thin (20–80 nm) films of stereoregular PMMA on a silicon wafer was measured via X-ray diffraction analysis [47]. This method allows weak density fluctuations to be estimated. It was shown that, in the polymer in contact with the substrate, density increases regardless of the polymer tacticity and film thickness. The observed effect was explained by a better packing of macromolecules at the interface due to the interfacial interaction and selective adsorption of stereoregular sequences.

The molecular dynamics of isotactic PMMA at 273–392 K was investigated with the use of dielectric spectroscopy [48]. Two loss peaks α and β were detected with β being independent of the film thickness and α corresponding to T_g of the polymer and decreasing with thickness by two orders of magnitude. At the same time, as evidenced by ellipsometry, T_g of the polymer gradually increases with a decrease in the thickness of the polymer layer. This contradiction in the character of change in T_g with a decrease in the film thickness, in accordance with [48], may be associated with different interactions between the polymer and the substrate. During dielectric-spectroscopy measurements of T_g, the film was placed between two aluminum electrodes, while in ellipsometry studies, the film was formed on a silica substrate.

Adsorption effects at the interface that entail restriction of the mobility of polymer chains may be so strong that they even cause an increase in the glass-transition temperature of the polymer. The behavior of PMMA adsorbed from a solution on a silicon wafer was studied with the aid of modulated DSC [40]. It was shown that T_g of the adsorbed PMMA increases from 108°C (T_g of the bulky polymer) to 136°C. There are other published data that, in thin (nanometer) polymer phases, an increase, rather than a decrease, in T_g occurs. For example, for nanosized species of polyacrylamide obtained via solution spraying on a solid surface, the value of T_g increased relative to that for the bulky polymer [49–51]. A similar effect was observed in microemulsions of PMMA [52–53].

For example, let us consider the data reported in [54]. Figure 5 plots the dependence of T_g of poly(bisphenol A hexane ether) on the thickness of its film on a silicon wafer. It is seen that T_g sharply increases at thicknesses less than 30 nm. Similar results were obtained during dielectric-relaxation spectroscopy measurements of T_g for polycarbonate based on bisphenol A. It was shown that, as the thickness of the PC film is decreased from 50 to 20 nm, its T_g increases from 420 to 443 K [55].

The above-described examples are in agreement with other data available for thin films on solid sub-

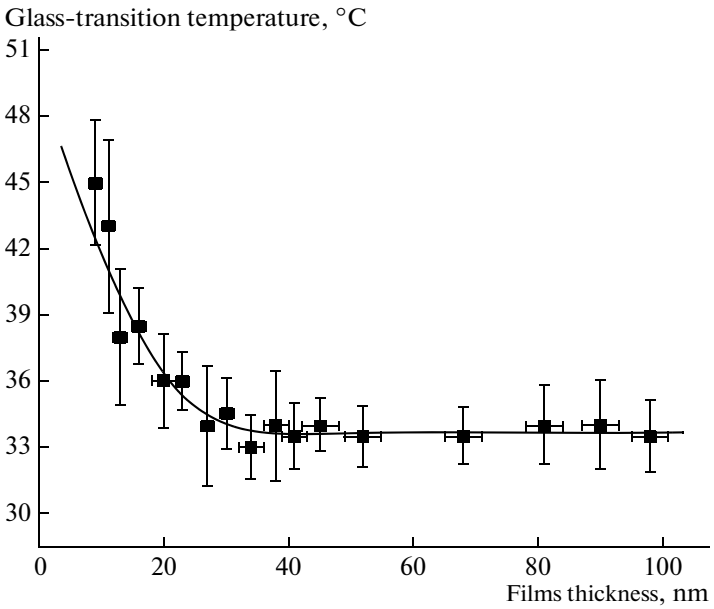

Fig. 5. Glass-transition temperature of poly(bisphenol A hexane ether) vs. thicknesses of its films deposited on the silicon wafer. The glass-transition temperature of the bulky polymer is 33.8°C [54].

strates in cases when there is a strong polymer–substrate interaction [56–59]. Hence, T_g of the polymer in thin films is not a constant value. It may decrease on a free surface or even increase if the polymer is in contact with the solid substrate, because of an intense interaction with the latter.

Moreover, the strong polymer–substrate molecular interaction in thin (nanometer) layers may fully suppress the large-scale mobility of the polymer. For example, the T_g value of the polymer (PS, poly(ethyl acrylate)) embedded in nanometer channels of zeolites cannot be measured via DSC [60, 61]. Nevertheless, for the individual polymer extracted from these channels with the use of a solvent, a T_g value typical for the bulky polymer is detected. As was shown in [62], despite very small diameters of channels (0.74 nm), macromolecules are efficiently sorbed by a zeolite probably via the reptation mechanism. Evidently, suppression of the molecular mobility of polymer chains responsible for glass transition is caused, first, by the narrowness of pores, in which the cooperative large-scale molecular motion is impossible, and, second, by the strong polymer–substrate interaction, which additionally suppresses the dynamics of polymer chains. Naturally, because of such impediments to the large-scale molecular motion, the crystallization of the polymer likewise becomes impossible under these conditions.

The above data demonstrating the effect of the sizes of the crystalline phase of the polymer on its T_g mostly refers to nanosized flat films and layers. However, this phenomenon is of a general pattern. As was shown recently in [63], the strongest depression in T_g of the polymer is observed in nanosized dispersions of the amorphous polymer (Fig. 6). As follows from Fig. 6, at diameters of nanoparticles less than 300–400 nm, there is the strongest depression of T_g of the polymer, which attains almost 60°C.

In summary of the foregoing evidence, it may be inferred that, in thin films and surface layers of amorphous polymers, the value of T_g decreases abruptly relative to the corresponding value of the bulky polymer. However, for thin (nanometer) films supported on solid substrates, the above-mentioned effect may become weaker or may even change sign owing to the interaction of the polymer with the substrate material (Fig. 5).

Note that, in fact, the effect of the geometric sizes of the polymer on its glass-transition temperature likewise strongly influences the temperature interval of its crystallization. As is generally agreed for linear polymers, the maximum rate of crystallization at a certain constant temperature is situated between the melting temperature and the glass-transition temperature of the polymer [64]. This relationship is related in particular to the features of nucleation during polymer crystallization. For both homogeneous and heterogeneous characters of nucleation, the temperature dependence of the rate of nucleation passes through a maximum at a temperature in the interval between T_g of the polymer (Fig. 7), below which the large-scale molecular motion necessary for nucleation is absent, and T_m, where the rate of nucleation is also zero [64, 65]. Evidently, the value of T_g shows a strong effect on the processes of polymer crystallization and determines the

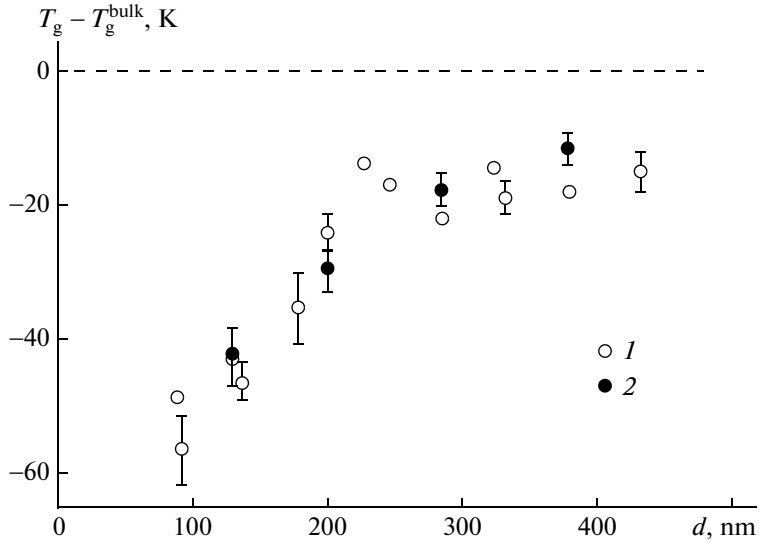

Fig. 6. Depression of glass-transition temperature ($T_g - T_g^{bulk}$) of PS nanoparticles measured via (*1*) DSC and (*2*) dilatometry vs. their sizes. The dotted curve corresponds to T_g of individual PS [63].

lower temperature boundary of its crystallization on the whole.

CRYSTALLIZATION OF POLYMERS UNDER CONDITIONS OF NANOMETER-SCALE SPACIAL RESTRICTIONS

To start, let us remember in brief some fundamental theses of crystallization in general. Crystals of a substance may appear on nuclei in a supercooled melt or via oversaturation of a solution of this substance. Nuclei may be large fluctuations of atoms (molecules) of this substance (homogeneous nucleation) or random species, for example, colloid particles, catalysts species, dust particles, and other admixtures able to adsorb crystallizable compounds on their surfaces (heterogeneous nucleation) [64, 66]. It is evident that the homogeneous nucleation requires much more pronounced supercooling, $\Delta T = T_m - T_{cr}$, where T_m is the melting temperature and T_{cr} is the crystallization temperature, than the heterogeneous nucleation.

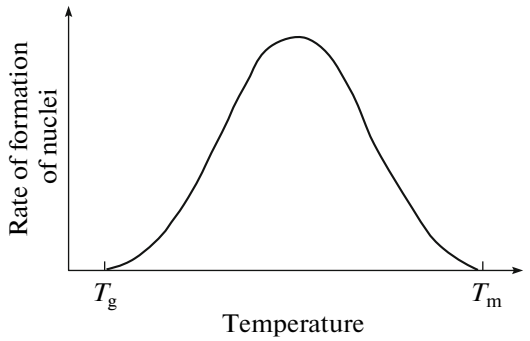

Fig. 7. Temperature dependence of the rate of formation of primary nuclei [64].

The above-described features of crystallization are of a general pattern, regardless of whether a low-molecular-mass compound or a polymer crystallizes. The linear structuring of polymer molecules is responsible for the specific features of polymer crystallization. The main distinct feature of the crystalline state of flexible-chain polymers is the folded character of their crystallites. Such crystallites, in which polymer chains are arranged into lamellas via repeated folding, serve as basic elements for more complex structures (spherulites, dendrimers, etc.). An important consequence of the folded structuring of polymer crystallites is that, as opposed to low-molecular-mass compounds, polymers always contain amorphous components; therefore, polymers are described in terms of the degree of crystallinity, which is usually in the range from 20 to 80%. Higher degrees of crystallinity in polymers are implemented rarely and require peculiar preparation conditions, which allow, for example, the growth of polymer single crystals [67] or extended-chain structures [68].

Polymer lamellas formed by folded macromolecules in various projections are schematically shown in Fig. 8 [69]. It is substantial that the value of folding in such lamellas is up to tens of nanometers, while their other faces are much larger. It is evident that the free surface energy of the side face formed by macromolecular folds, σ_1, is much greater than the free surface energy of the face plane formed by densely packed mutually oriented macromolecules, σ_2 [69].

During crystallization in the bulk, anisotropic lamellas may be isotropically (chaotically) oriented in

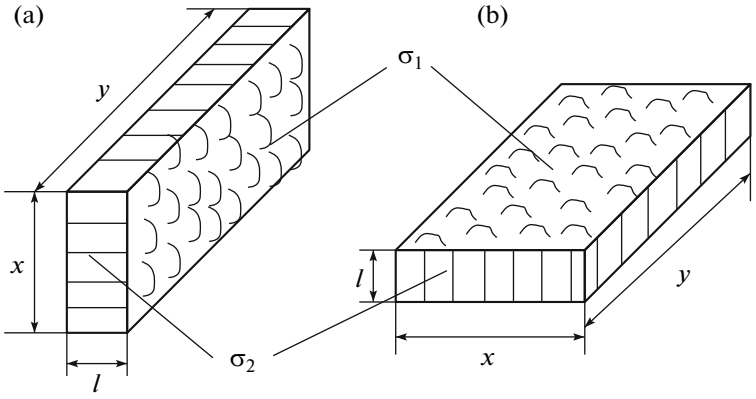

Fig. 8. Schematic representation of crystalline polymer lamellas built up via folding of macromolecules: (a) edge-on orientation of the lamella relative to the substrate and (b) flat-on orientation of the lamella relative to the substrate [69]. Lamella plane x–y is formed by folds of macromolecules. Planes l–x denote edge faces of the lamella. Straight lines on faces indicate the directions of c axes of macromolecules.

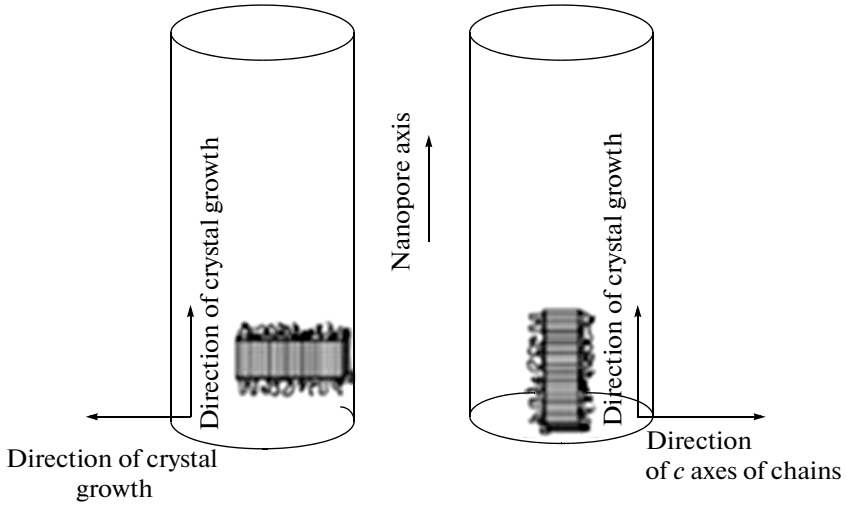

Fig. 9. Possible directions of crystallite growth and the orientation of c axes in nanosized cylindrical pores [70].

space. However, the lamella cannot freely rotate in systems with nanosized restrictions commensurable with its thickness. As a result, the preferred orientation of lamellas is observed, as experimentally verified in many studies for thin films, block copolymers, and nanoporous materials.

As an example, Fig. 9 [70] shows possible directions of growth of crystals and their orientation in cylindrical pores. Crystals may grow both in the direction of the pore axis and normally to this direction. There are mostly two types of preferred orientations: perpendicular (edge-on lamellas) and parallel (flat-on lamellas) orientations of the alignment of lamella with respect to the flat surface of the substrate or the walls of pores in the cylindrical pore. It is clear that a decrease in the volume of the crystalline polymer phase to the nanolevel inevitably affects both the sizes of crystalline lamellas and their orientation in cases when spatial restrictions are of an asymmetric geometry. Figure 8 shows two types of orientation of crystalline lamellas relative to the flat substrate. Moreover, the above-mentioned great difference in surface energies of various faces of polymer folded crystallites should inevitably affect both crystallization of the polymer on the whole and the orientation of crystallites in the resulting material.

The above-described features (difference) of the molecular motion of the polymer, for which T_g is a measure at the boundary with air or with the solid substrate, transform this seemingly simple and well-studied system as a thin polymer film on the solid substrate into a very nonsimple object. Let us examine a thin polymer film deposited on a solid substrate (Fig. 10) [54].

As is clear from Fig. 10, the properties of the surface of a polymer film facing air (e.g., T_g) are different from those of the surface in contact with the solid sub-

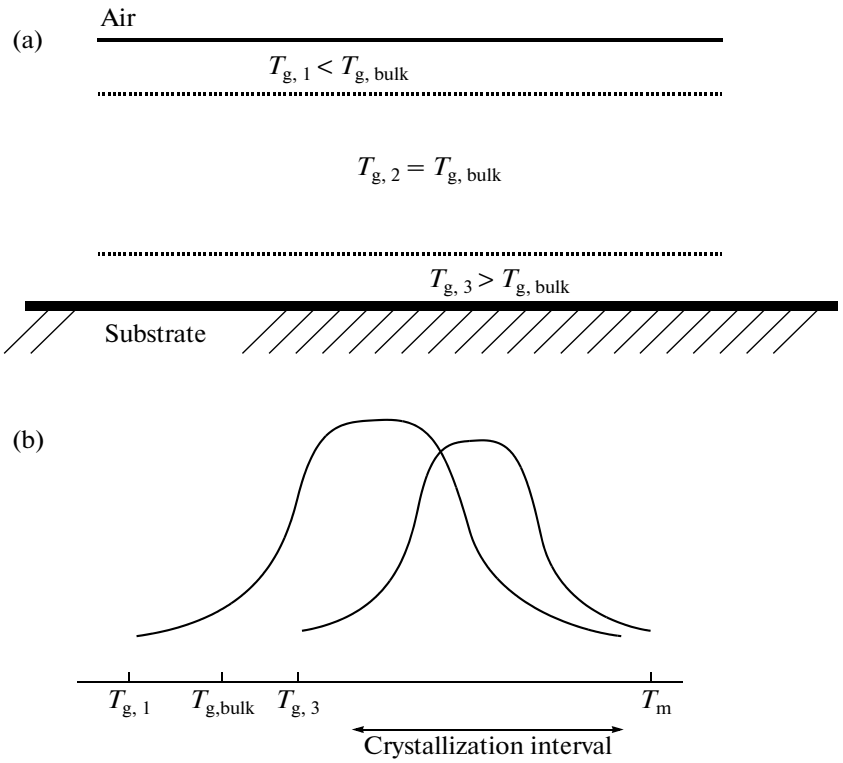

Fig. 10. (a) Schematic representation of the three-layer model of a thin polymer film on a solid substrate and (b) schematic representation of the temperature dependence of the nucleation rate for the polymer adjoining the solid substrate and having an increased glass-transition temperature (T_g, 3) relative to that of the bulky polymer and for the polymer occurring in the surface layer facing air and having a decreased glass-transition temperature ($T_{g,1}$). The glass-transition temperature of the bulky polymer ($T_{g,bulk}$) is shown between these temperatures [54].

strate. This circumstance strongly influences crystallization of the polymer and, in particular, the temperature interval of its crystallization.

The three-layer structural model of polymer films on a solid substrate (Fig. 10) makes it possible, in particular, to gain an understanding of the orientation effects existing during crystallization. A high molecular mobility and a low density of the polymer at the film/air interface determine a strong tendency toward orientation of the *c* axes of macromolecules parallel to the film surface; that is, conditions appear for the formation of crystallites with the edge-on orientation of the lamella relative to the free surface of the film [71–74]. It is important that the above-mentioned high molecular mobility in the surface layer of the polymer relative to that of the layer contacting the solid substrate provides a higher rate of nucleation during its crystallization. After the formation of crystallites with the edge-on orientation of lamellas, the latter may propagate in directions both parallel and normal to the surface. The defects of crystals—such as extended loops not included in the crystal lattice, cilia, and screw dislocations—are the direct causes of lamella branching [75–82]. The existence of these defects in the nucleated crystallites easily give rise to lamellas having the flat-on orientation relative to the substrate, as is schematically shown in Fig. 11 [54].

As was found in [83], when the polymer film is thicker than 1000 nm, its crystallization occurs via the edge-on orientation of the lamella relative to the substrate; that is, *c* axes are arranged parallel to the substrate surface. When the thickness of the film is lesser, the system demonstrates the flat-on orientation of the lamella relative to the substrate; that is, *c* axes are arranged normally to the substrate surface.

The Monte Carlo simulation of crystallization in thin polymer films shows [84] that, at high temperatures, crystallization in thin polymer films proceeds with the edge-on orientation of lamellas relative to the substrate in the case of an inert (repulsing) substrate and largely with the flat-on orientation of the lamella with respect to the substrate if interaction between the polymer and the substrate is good.

The multilayer structure of the thin polymer film was experimentally observed in [85] with the use of the fluorescence technique, in which a thin layer of fluorescent PS is included into an unlabeled PS film. As a result, the authors managed to measure local T_g values in various polymer layers remote from the surfaces to different extents. The glass-transition temperature of

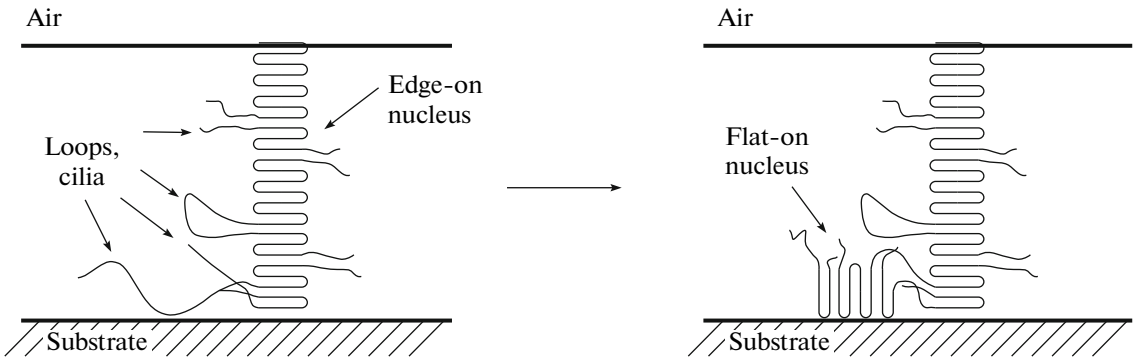

Fig. 11. Schemes illustrating (left) the edge-on orientation of the lamella relative to the substrate at the first stage of nucleation during crystallization of the polymer film on the solid substrate and (right) growth of the lamella leading to the appearance of the flat-on orientation of the lamella relative to the substrate [54].

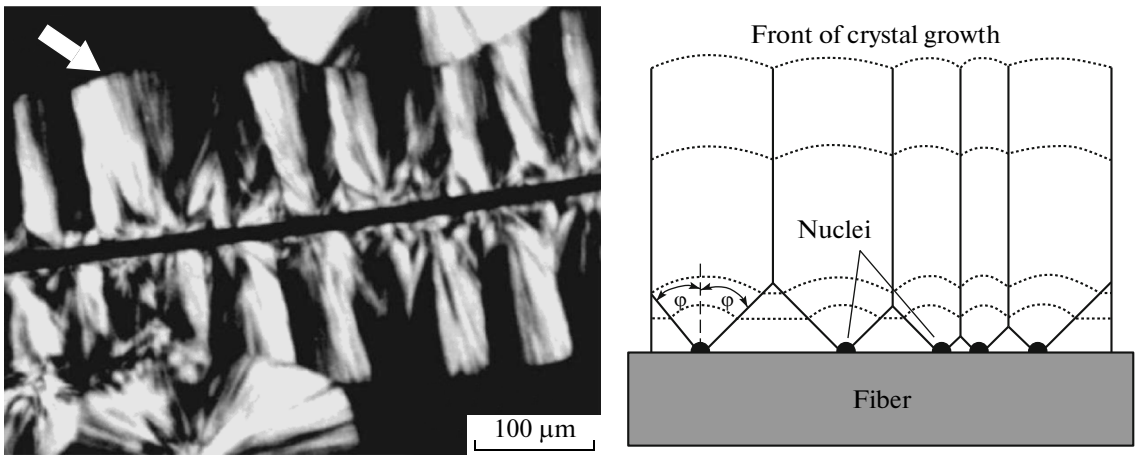

Fig. 12. (Left) Optical micrograph imaging the growth of the transcrystallite zone of isotactic PP on the carbon fiber (the black band at the center of the picture) and (right) schematic representation of nucleation of crystals on the fiber and their growth [86].

the fluorescent polymer placed on the surface of the bulky polymer decreases abruptly with the thickness of the fluorescently-labeled layer. The glass-transition temperature of the fluorescent layer depends on its location in the film. If this layer is covered with unlabeled PS with a thickness above 18–30 nm, it features the bulk T_g. At a smaller thickness of the covering layer, T_g of the fluorescently-labeled PS decreases relative to that of the bulk. The decrease tends to increase with a decrease in the thickness of the covering layer. In accordance with the authors of [85], the given behavior may be described in terms of the two- or three-layer model.

Hence, the orientation of crystallites in the thin film of the crystallizable polymer on the substrate is determined by the mobility of polymer chains as well as the temperature and interaction between the polymer and the substrate.

Role of Surface Curvature in Polymer Crystallization on the Interfacial Surface

In the previous section, the crystallization of polymers on a flat surface was discussed. There is another factor able to affect the molecular mobility and T_g of the polymer and, hence, its crystallization in thin layers. Even in the absence of good interaction with the substrate, the intermolecular mobility of the polymer may decrease substantially (while T_g increases) if a particle (polymer phase) occurs in a certain cage (cavity) on the substrate surface [37–39]. This steric effect, which, in fact, reflects the effect of perfection and curvature of substrate surface, has been studied in depth [23].

Composites filled with nanofibers or nanotubes are most suitable for studying the effect of surface curvature on the crystallization of polymers. In these cases, the polymer layer close to the fiber surface crystallizes as a rule so that macromolecules are oriented parallel to (along) the fiber axis by their *c* axes. This specific

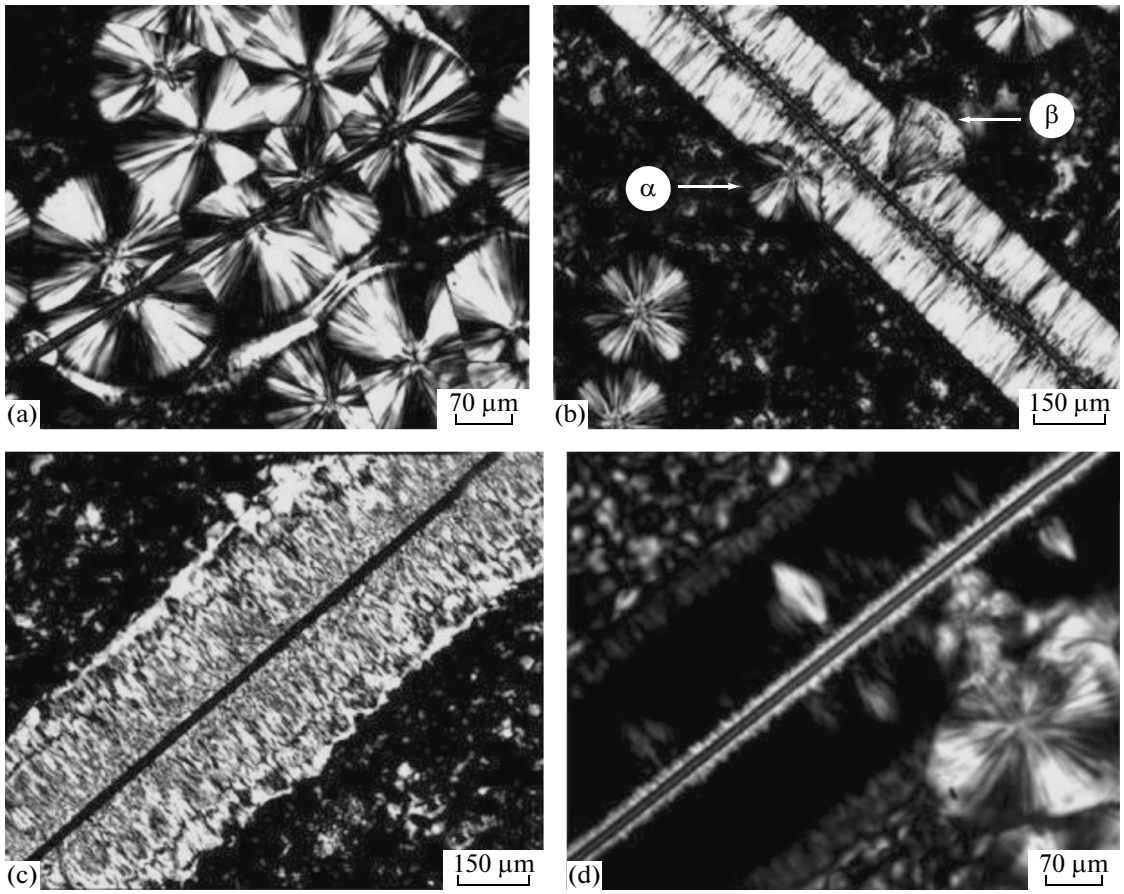

Fig. 13. Optical micrograph showing the morphology of the isotactic PP–Kevlar 49 system. The samples were stretched at a rate of 30 μm/s for (a) 0, (b) 20, and (c) 60 s; (d) the selective melting of isotactic PP at 158°C [97].

structure is formed because of a high density of nuclei on the fiber surface, which hampers the development of spherulites and other complex crystalline forms and forces crystals to grow in one direction normal to the fiber axis. This situation is illustrated by Fig. 12 [86].

There are several factors that govern this transcrystallization. First, an important role is played by the structure of the fiber surface. For example, aramid fibers and high-modulus carbon fibers can induce the transcrystallization of isotactic PP, whereas glass fibers and fibers based on a high-strength carbon fiber have no effect on its crystallization [87]. It was shown that high-energy surfaces may enhance the density of nuclei on the surface and thus may facilitate the formation of transcrystals on the surface [88, 89].

Second, the presence of interfacial stresses or a temperature gradient at the interface is likewise favorable for the development of the transcrystallization layer [90, 91].

Third, the presence of viscous flow, which frequently accompanies fiber formation, is another important factor of nucleation and orientation of the polymer on the fiber surface. Under shear, transcrystallization always occurs, regardless of the type of surface. This situation was best illustrated for crystallization of PP in the system PP–fiber that was stretched along the long axis [92–96]. For example, it was found [97] that a Kevlar 49-based fiber does not contribute to the nucleation of PP transcrystals on it (Fig. 13a) and that crystallization gives rise to spherulites in the monoclinic alpha form. However, the oriented columnar structures of PP were always observed in the vicinity of the Kevlar fiber if it was stretched along its axis (Figs. 13b, 13c), although these structures could be different, depending on the rate or time of stretching. This outcome is additionally confirmed by experiments on the selective melting of β crystals of isotactic PP at 158°C (Fig. 13d).

Moreover, if the fiber occurs in the crystalline state, it provides another kind of transcrystallization (via the epitaxy mechanism). For example, there is a correspondence between the crystal lattices of nylon and isotactic PP with a high-modulus carbon fiber, which leads to the transcrystallization of nylon and PP on its surface [98]. When a fiber and a matrix are based on the same polymer, transcrystallization proceeds owing to the identical chemical compositions and perfect fit of the crystal lattices [88, 99–103].

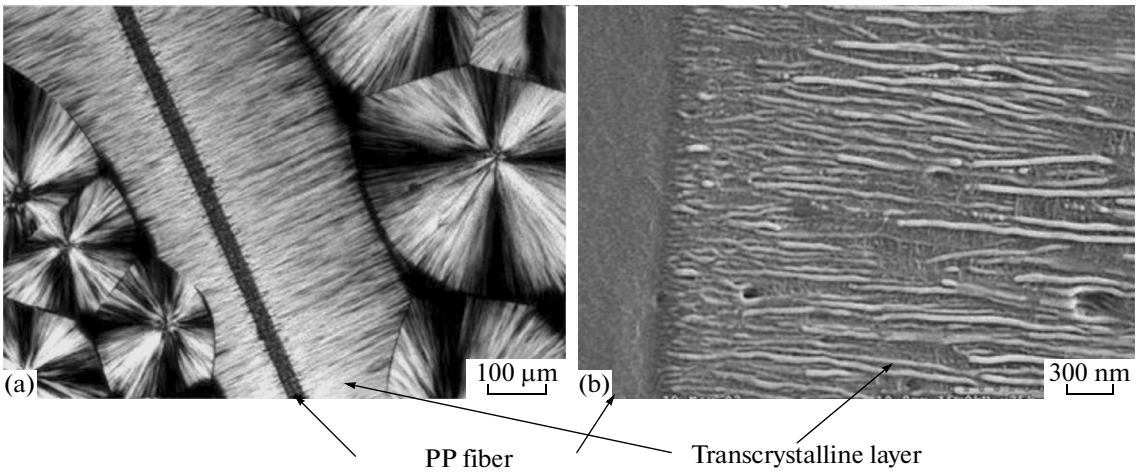

Fig. 14. (a) Optical micrograph showing the growing layer of PP on the surface of a PP fiber [101] and (b) SEM micrograph of the transcrystalline layer [99]. The sample was obtained via placing of the PP fiber in a supercooled melt of PP at 137°C followed by isothermal crystallization over 6 h.

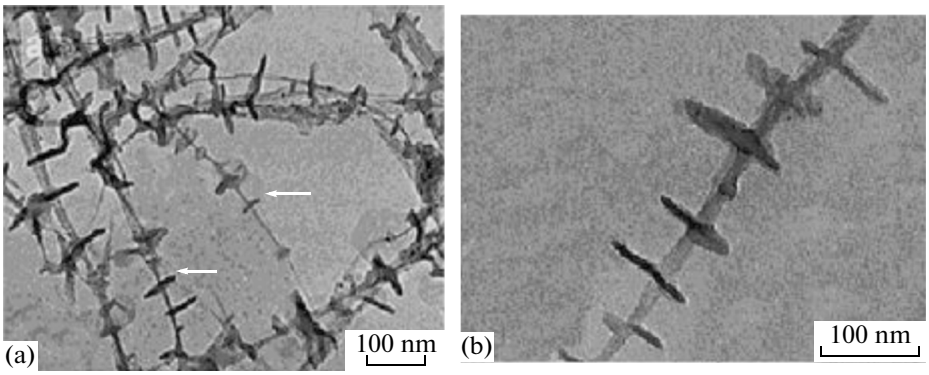

Fig. 15. Electron micrographs of PE crystalline structures on the surfaces of CNTs [114].

As an example, Fig. 14 shows the morphology of PP crystallized on the surface of a PP fiber [101].

As is clear from the comparison of Figs. 12 and 14, the amounts of nuclei on the surfaces of PP and carbon fiber are different. On the carbon fiber, the growth of crystals along the fiber is confined by nuclei; therefore, the front of transcrystallites propagates deep into the melt, while on the PP fiber, it is not confined by anything; simply each lamella gives rise to the onset of transcrystal growth in the direction normal to the fiber axis. For composites based on the same polymer as a matrix and a fiber, a unique behavior may be observed because of closeness of their melting temperatures. The surface of the fiber may be partially molten; therefore, PP crystallizes in the β form [99–103].

In recent years, nanofibers and nanotubes having high surface-to-volume ratios have attracted considerable attention as nucleating agents [104–109]. Owing to the high value of this ratio, similar objects initiate crystallization that is quite different from crystallization on the surface of a common fiber and the behaviors of polymers during crystallization around nanofibers and nanotubes are quite different. The role of carbon nanotubes (CNTs) was examined in detail in review [109]. CNTs were found to be highly efficient as nucleating agents for PP [110]. In this case, the transcrystallization of PP occurs on the surface of a CNT in the flat-on form with the orientation of molecular chains normal to the long axis of the CNT. Furthermore, the CNT may initiate the crystallization of PP in a less stable β form [111].

As was shown in a number of studies, CNTs very efficiently initiate the development of transcrystals in various polymers and the orientations of transcrystallites may be different, as generalized in [112]. In [113–115], crystallization of the polymers on CNTs from solutions was investigated. Under controllable conditions, disklike edge-on oriented lamellar crystals growing on the surfaces of CNTs may be prepared.

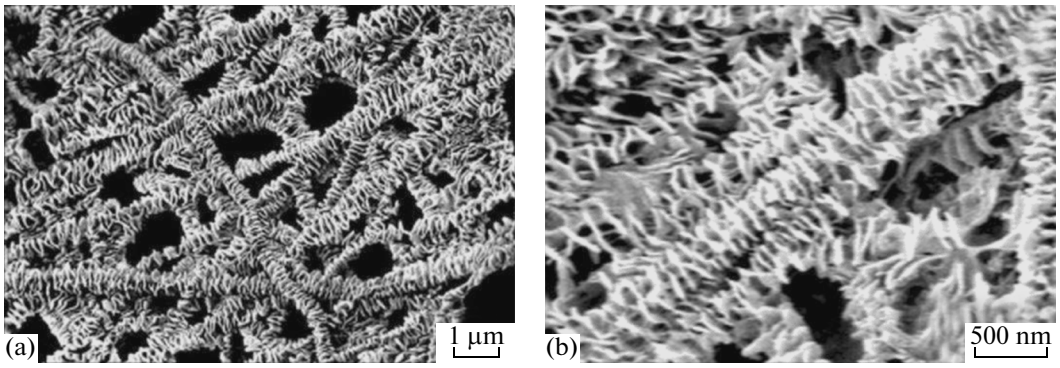

Fig. 16. Electron micrographs of ultrahigh-molecular-mass PE having the shish-kebab structure that were taken at various magnifications [121].

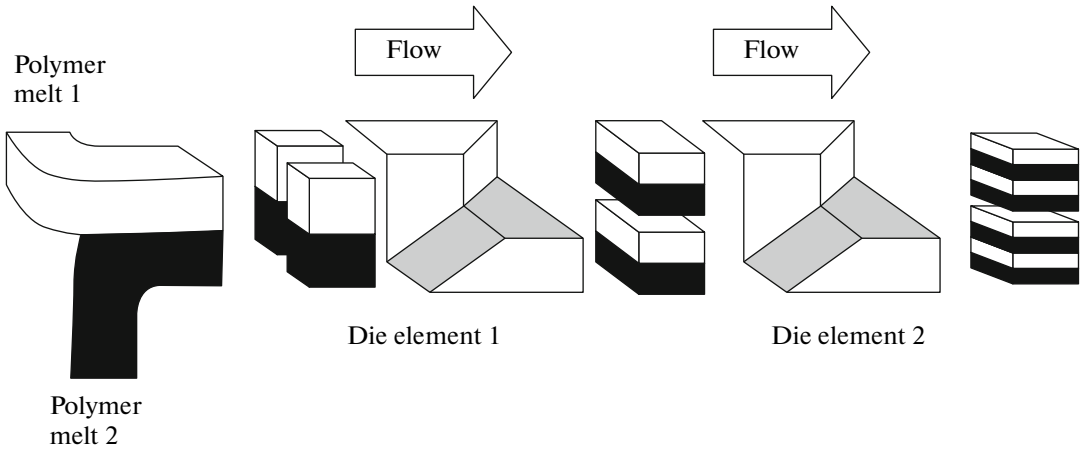

Fig. 17. Schematic representation of the device for coextrusion of melts that allows the force assembly of nanolayer filmed based on immiscible polymer pairs to be performed. The initial stage of preparing films containing from 2 to 8 layers is shown [125].

Figure 15 illustrates such structures grown from PE solutions [114]. Similar structures were grown on CNTs from polymer solutions in supercritical CO_2 [116–120]. In these structures, lamellar crystals were regularly arranged along CNTs with the orthogonal orientation between the surface of the polymer lamella and the axis of the CNT. The periodicity of lamellar crystals along the CNT axis is governed by the conditions of crystallization, such as the concentration of the solution, the temperature of crystallization, and the type of solvent. The mechanism of CNT-induced crystallization is apparently the same as that in carbon-filled plastics. At the same time, with consideration for the very small sizes of CNTs, it may be assumed that the nanotube itself plays the role of a macromolecule, thereby leading to the preferred stacking of chains along its main axis [113]. Figure 16 demonstrates that the structure of the polymer is similar to the shish-kebab structure that appears in stretched or sheared melts (solutions) [121–123].

The formation of the shish-kebab structure is a kind of surface-induced epitaxy of the polymer, in which a picket fence of folded-chain lamellas is formed around preliminarily stacked long (unfolded) chains of the central part. This situation was convincingly demonstrated via modeling of this process [124].

Thus, the geometric features of the solid substrate on which crystallization of the polymer is performed have a strong effect both on the process of crystallization and the structure and properties of the final product. The effect of substrate geometry is especially pronounced at the stage of nucleation of crystallization.

Multilayer Polymer Nanosystems

The features of polymer crystallization on interfacial boundaries have been considered in brief. As was noted above, under these conditions, crystallization is in fact confined, although, in this case, geometric restrictions act in one direction solely. It is evident that the above-discussed features of polymer crystallization on interfacial boundaries will manifest themselves more intensely and distinctly in cases when the layer of the crystallizable polymer is in contact with the substrate from both sides, for example, in multilayer films.

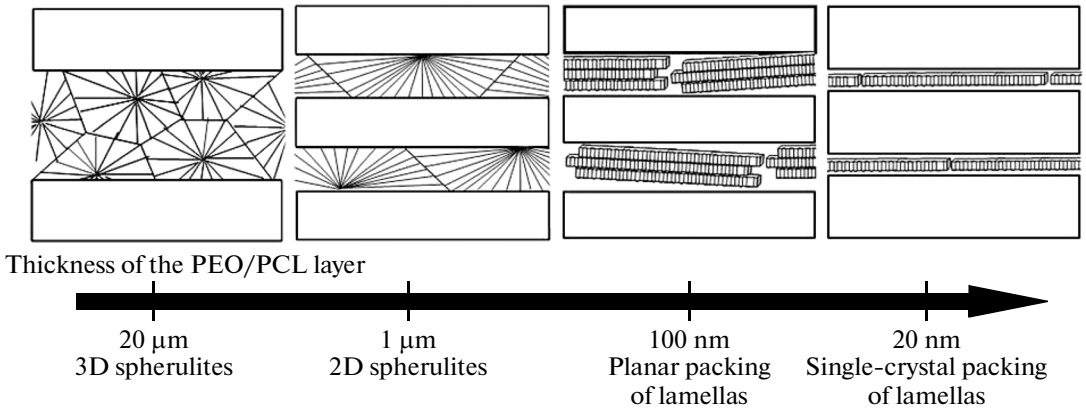

Fig. 18. Structural evolution of PEO and PCL crystalline layers with their thicknesses in multilayer films based on the above polymers and PS [126].

Therefore, the method of the so-called force assembly of multilayer polymer systems appears to be very efficient [125, 126]. The process of layer multiplication relies on the viscoelastic origin of polymer melts during their coextrusion, which leads to a successive increase in the amount of layers of immiscible polymers in the resulting film. Figure 17 schematically represents the device for such an assembly. A system of N sequences of dies yields an amount of layers in the film equal to $2^{(N+1)}$.

A typical amount of layers is hundreds, and the total thickness of the multilayer film is on the order of 1 μm. Recent progress in multilayer coextrusion has made it possible to decrease the thicknesses of layers by two orders of magnitude, from the microscale to the nanoscale [127]. Nanolayer films consisting of thousands of continuous layers based on two immiscible polymers with a thickness of each layer less being than 10 nm were prepared.

Apparently, if even one of the components in this system is based on a crystallizable polymer, it is very easy and efficient to study its crystallization in layers with practically any thicknesses. Note that, as opposed to the case of films deposited on the solid substrate considered in previous sections, the multilayer-coextrusion procedure makes it possible to prepare and to investigate superfine layers of a crystallizable polymer confined by another polymer layer from both sides.

In [126], the crystallization of two polymers—poly(ethylene oxide) [128] and poly(ε-caprolactone) (PCL) [129]—in multilayer films based on these polymers and atactic (amorphous) PS was analyzed. Both systems have much in common in their structures and in their dependences on layer thicknesses (Fig. 18). At layer thicknesses above 10 μm, both polymers are composed of traditional three-dimensional spherulites. At a thickness of 1 μm or less, two-dimensional spherulites (discoids) are formed. A further decrease in the thicknesses of layers (down to 100 nm) leads to crystallization of the polymer in the form of individual mutually oriented lamellas, while at layer thicknesses on the order of 10 nm or less, structures similar to the single-crystal structure are formed.

Along with layer thicknesses, the morphology of crystals in the nanometer films is strongly influenced by the crystallization temperature. Because both polymers (PEO and PCL) feature low T_m values (65 and 57°C), the effect of T_{cr} values of polymers in nanosized spatial restrictions on their morphology under conditions when the confining PS layers remain glassy may be investigated.

A change in T_{cr} has a strong effect on crystallization in both systems. At low values of T_{cr}, the edge-on orientation of the lamella relative to the substrate is implemented in both cases. When T_{cr} increases, there is the appearance of transition regions where, for PEO and PCL, the transition of the edge-on orientation of lamellas relative to the substrate to the flat-on orientation occurs. The temperature interval of this transition

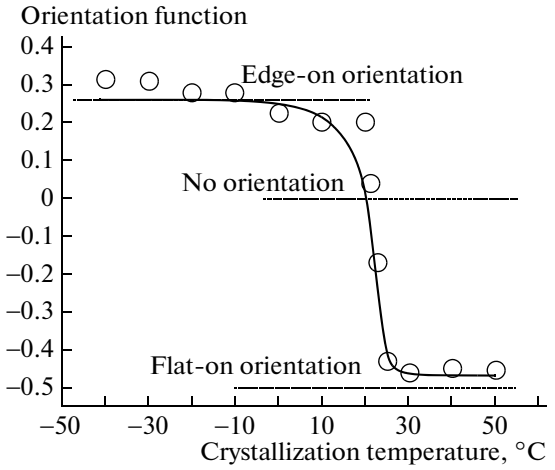

Fig. 19. Plot of Herman's orientation function [126] vs. crystallization temperature of PEO.

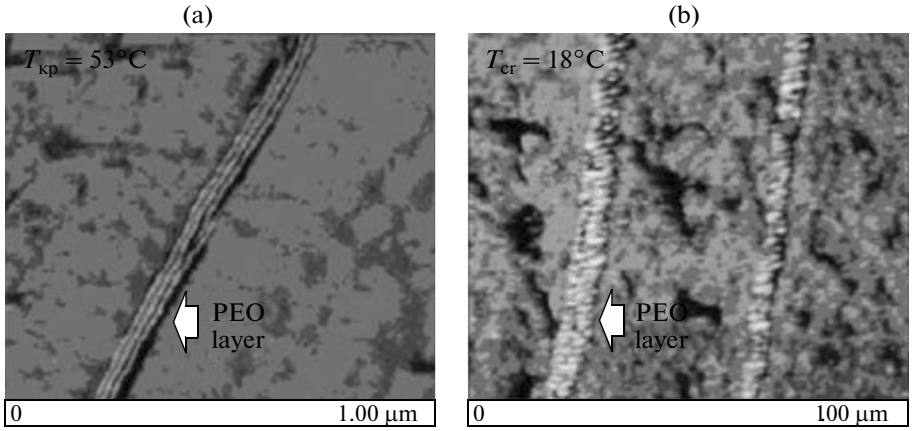

Fig. 20. AFM images of the cross section of the PEO/PS multilayer film with a PEO layer with a thickness of 75 nm: (a) PEO was molten at 90°C and crystallized at 53°C (lamellas oriented parallel to the layer), and (b) PEO was molten at 90°C and crystallized at 18°C (lamellas oriented perpendicularly to the layer) [126].

is narrow (Fig. 19). Figure 19 shows the dependence of the orientation function [126] derived from the azimuthal distribution of intensity of WAXS scattering for the reflection of PEO (120) on the crystallization temperature. It is well seen that the transition from one type of orientation of PEO crystals to the other occurs in the temperature interval ~5°C and occurs through the stage of absence of any orientation.

A similar change in the orientation of lamellas with an increase in T_{cr} supposes a strong effect of crystallization kinetics on the orientation of crystals in nanolayers. The confining PS layers, in accordance with [126], play a crucial role in nucleation. PS is an amorphous polymer; therefore, the epitaxial crystallization of PEO and PCL on the surface of PS is excluded. However, it was proposed that there is a preferred orientation of PEO and PCL macromolecules on the surface of PS; as a consequence, homogeneous nucleation is facilitated. During homogeneous nucleation in the bulk, T_{cr} of PEO is in the range from –10 to 0°C. In contrast, nanolayers of PEO crystals with the edge-on orientation of lamellas were obtained at much higher temperatures (up to 20°C). A further increase in T_{cr} levels off the role of surface nucleation, and the crystals grow on heterogeneous nuclei. Because the amount of heterogeneous nuclei in nanolayers is small, the growth of lamellas occurs in the plane of the layer; as a result, their flat-on orientation develops.

Atomic-force microscopy clearly demonstrates these two types of orientation in multilayer PEO–PS films in PEO 75-nm-thick layers crystallized at two different temperatures (Fig. 20) [126].

In addition, geometric restrictions exert a considerable effect on the kinetics of crystallization of the polymer. During the crystallization of PEO and PCL in 25- to 50-nm-thick layers, the rate constants of crystallization (in the Avrami equation) decrease by an order of magnitude relative to the corresponding value for the bulky material [129, 130]. In this case, crystallization occurred via the heterogeneous nucleation even in layers with thicknesses of 25 nm. Avrami exponent n, describing the geometry of crystal growth in layers with thicknesses of 25–50 nm, is 2.0 for both polymers. This fact is evidence for the two-dimensional growth of crystals in these systems (as opposed to in the bulk, where the growth of crystals is three-dimensional).

In summary of the foregoing, it may be inferred that the force-assembly method of multilayer polymer systems is an efficient tool for studying various properties of polymers and their crystallization, in particular in layers of practically any sizes. The effect of various factors on phase transitions in polymers was revealed by this method; for details, see the publications of E. Baer et al. [126, 131].

Crystallization of Polymers in Interplanar Cavities of Layered Nanosilicates

In the previous section, the method of creating multilayer polymer composites with layers of various thicknesses down to nanosizes was considered. There is at least one more possibility to implement and study crystallization of polymers in nanometer layers. The case in point is layered nanosilicates that contain nanometer-scale interplanar cavities. This circumstance is responsible for the wide use of layered silicates for the manufacture of a wide variety of organic–inorganic nanocomposites. Filling (intercalation) of interplanar cavities of silicates with various polymers provides a real opportunity to produce a great diversity of new materials [132, 133].

Nanocomposites based on layered silicates are characterized by higher Young's moduli [134–137], reduced temperature coefficients of thermal expansion [134, 135], decreased gas permeabilities [134–137], enhanced swelling resistances [138], ionic conductivities [139–141], etc. In this context, it is no

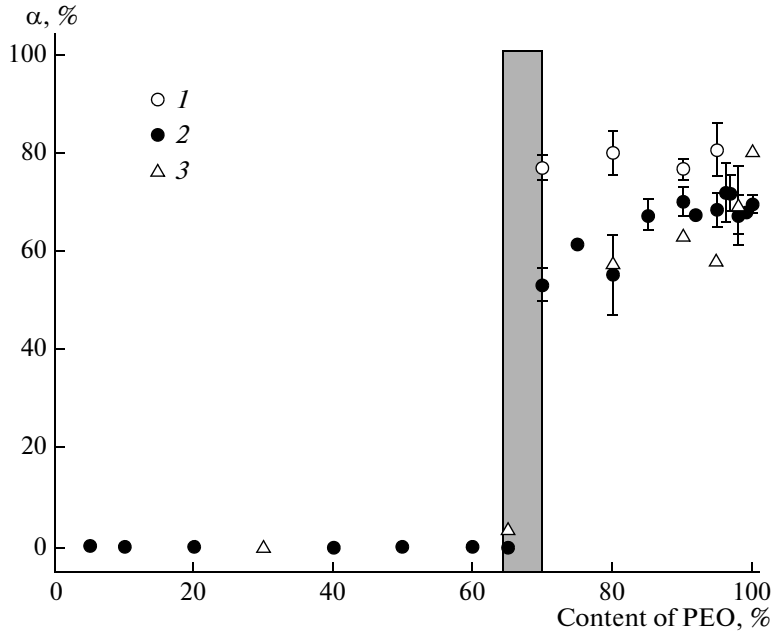

Fig. 21. Degree of crystallinity of PEO vs. its content in montmorillonite according to (*1*) X-ray diffraction, (*2*) DSC, and (*3*) Raman spectroscopy [154].

wonder that the preparation of organic–inorganic systems based on nanolayered silicates evolved long ago to form a separate area of physical chemistry of polymer materials science, and important surveys concerning this issue are available in the literature [132, 133].

Mixing of layered inorganic materials with a polymer may give rise to three different structures, depending on the specific interactions between components [142,143]: (i) phase separation, when components are immiscible, (ii) intercalation, when polymer chains appear in the interlayer space with a thickness of 0.8–2.5 nm, and (iii) exfoliation, when the interaction between chains and surfaces is so strong that the layered structure of the inorganic material is destroyed and dispersed into platelets (silicate layers).

It is necessary, even if in brief, to touch upon the issue of crystallization of polymers in the nanosized interlayer space of silicates. Above all, it is important to establish the fact of penetration of polymer molecules into such narrow pores. Here it should be emphasized that in many cases, for example for PS [144–146], PEO [139], and PDMS [138], intercalation occurs via melting at abnormally high rates (over time on the order of 5 min). In this case, polymer chains having diameters of the statistical coil of about 10 nm rapidly and very efficiently diffuse into slits 1 nm in size.

The above data correlate with the results reported in [147, 148], in which a more intense molecular mobility of the polymer in nanometer layers of the layered silicate was revealed. It was shown that, when polymer molecules are intercalated between two solid surfaces separated by 1.5–2.0 nm, their segmental mobilities are higher than those in the bulk [147, 148]. This dynamics of the polymer confined within the layered nanosilicate is similar to the relaxation behavior of small molecules confined within nanopores, for which the T_g values decrease with a decrease in the pore size [149–153].

In [154], PEO was intercalated in various amounts in montmorillonite and then its crystallization in such confined volumes was studied. It was shown that, at the initial stages of filling of nanopores, PEO does not crystallize in the layered silicate (Fig. 21). When the amount of PEO is increased (above 60%), its intense crystallization begins and the degree of crystallinity tends to grow with an increase in the amount of the polymer in the system. It is supposed that the penetration of PEO into such narrow pores fully suppresses its crystallization. However, after filling the interplanar cavities, the polymer localizes in the remaining unoccupied space of the nanosilicate, where its crystallization is not hampered and its degree of crystallinity increases abruptly (in a jumplike manner) (Fig. 21) [154].

In conclusion of this section, note that the mechanism of phase transitions of polymers in the interlayer spaces of nanosilicates is still vague and studies in this direction persist.

Nanoporous Cylindrical Templates

The publications considered above address the processes of crystallization of polymers in nanosized spaces having the geometries of flat layers. At the same

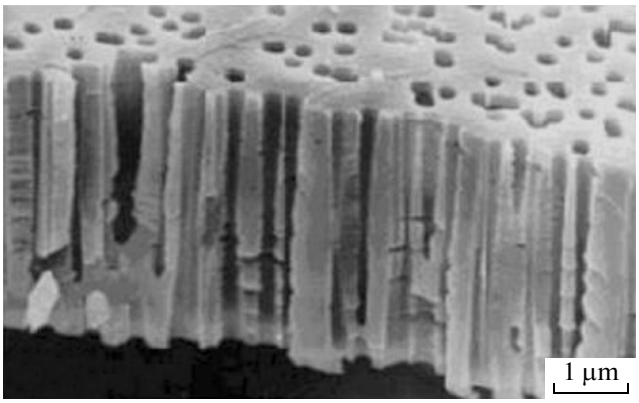

Fig. 22. Typical structure of a polymer track membrane [155].

time, studies dealing with the phase transitions of polymers in templates with the geometry of rectilinear nanocylinders arranged in parallel to each other in rigid matrixes have been developed vigorously in recent years.

There are two types of rigid templates with uniformly sized cylindrical pores on the nanometer scale: nuclear filters (track membranes) and aluminum oxide plates. Track membranes [155, 156] are obtained via irradiation of polymer films with heavy-metal ions followed by chemical etching of the resulting tracks. As a result of this treatment, polymer layers (films) penetrated by cylindrical channels arranged in parallel appear, with their amount and diameters being varied in a wide range (Fig. 22).

The second type of membrane is formed by rigid templates based on nanoporous aluminum-oxide plates that are prepared via the electrochemical anodization of aluminum templates. This method has been known for a long time and has been highlighted in length in the literature [157, 158].

Figure 23 shows micrographs of several templates with various diameters of cylindrical channels [159]. It is important that their preparation technique makes it possible to obtain both randomly arranged and regularly arranged (with hexagonal packing) cylindrical channels in AOPs [156, 157, 160]. As is seen, regularity in the arrangement of channels may be attained for practically any diameter of channels in AOPs.

In [161–163], AOPs were used for the first time to ascertain the effect of nanometer-scale spatial restrictions on the crystallization of polymers. For this purpose, the polymer was either synthesized within the template membrane or introduced in pores from polymer melts and solutions via wetting [164, 165]. The ambient pressure may likewise be the driving forces of polymer introduction in nanopores [166]. Nanoporous aluminum templates filled with the polymer melt (solution) dissolve readily, for example in alkalis; as a

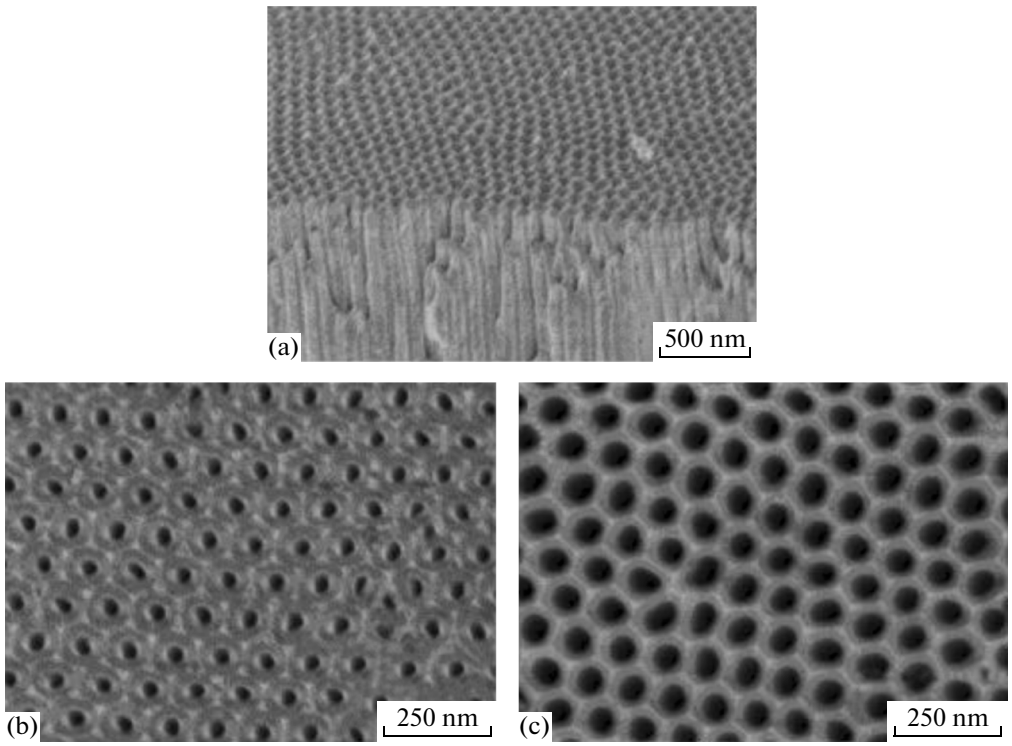

Fig. 23. SEM micrographs of templates based on aluminum oxide plates with diameters of cylindrical channels of (a, b) 35 and (c) 65 nm; (a) side view, and (b, c) outer-surface view [159].

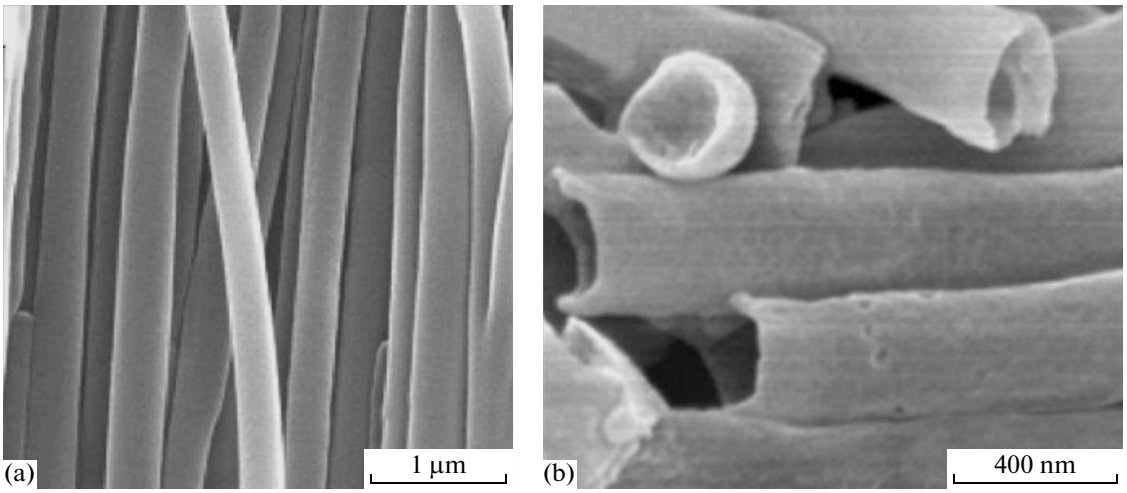

Fig. 24. SEM micrographs of (a) nanorods derived from syndiotactic PS [167] and (b) PVDF nanotubes [168] prepared via filling of the aluminum porous matrix with (a) syndiotactic PS melt and (b) a PVF solution in DMF followed by dissolution of the matrix based on aluminum oxide plates.

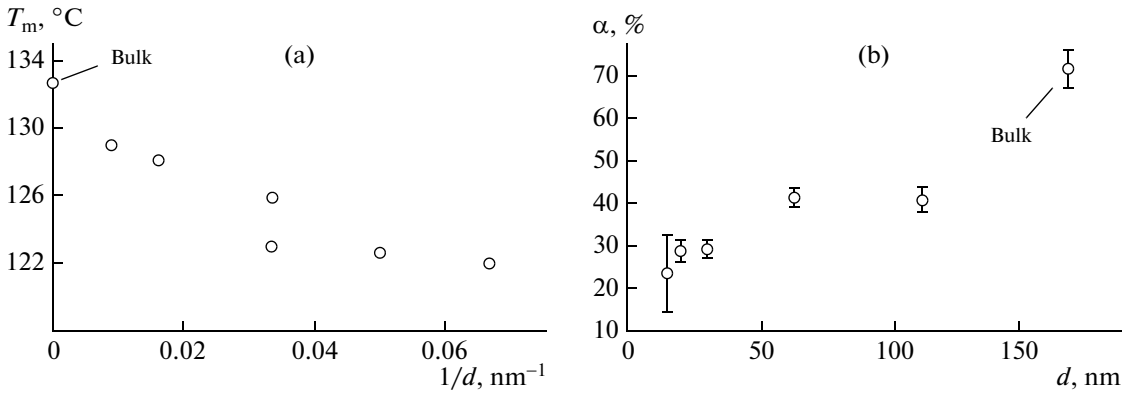

Fig. 25. (a) Melting temperature of linear PE and (b) its degree of crystallinity vs. the diameters of pores in the aluminum template in which crystallization and melting occur [169].

result, the polymer may be prepared in the form of nanorods (nanowires) or nanotubes (Fig. 24).

Figure 24 shows the products that allow the properties of polymer in the nanostate to be investigated. The properties of such nanoobjects were the subject of many studies and, at present, vast information has been accumulated and generalized in reviews [157, 158].

For example, nanorods derived from syndiotactic PS do not manifest molecular orientation in the molten state in cylindrical pores of the aluminum matrix [167]. When the amorphous syndiotactic PS is heated in the solid state from room temperature, it crystallizes in nanorods and, as in the bulk, forms the α form of crystals with the same degrees of crystallinity and without any preferred orientation. In contrast, when the syndiotactic PS crystallizes from the melt directly in nanopores, it forms the β form with the *c* axis oriented normally to the nanorod axis. The crystallinity of the polymer in such nanorods is much lower than that in the bulk; the smaller the sizes of pores, the lower the crystallinity. This behavior may be explained by a change in the rate of nucleation, which is high when crystallization occurs during heating from room temperature and low when crystallization occurs during melt cooling.

In [168], AOPs were used to gain insight into the effect of spatial restrictions on the crystallization of linear PE. Figure 25 demonstrates the effect of nanopore sizes on melting temperature T_m and the degree of crystallinity of the polymer. It is well seen that the sizes of the PE phase drastically affect both the melting temperature of the polymer (Fig. 25a) and its degree of crystallinity (Fig. 25b).

The thermal characteristics of PEO in the form of nanotubes with a wall thickness of ~100 nm were stud-

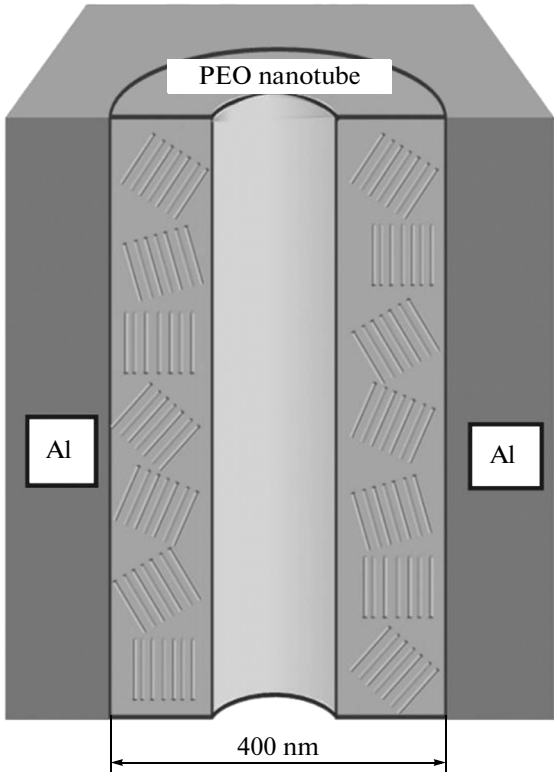

Fig. 26. Schematic image of the PEO nanotube in the aluminum cylindrical matrix [170].

ied in [169]. The nanotubes were prepared via soaking of aluminum templates having 400-nm-dia cylindrical pores with a PEO solution or melt. Soaking conditions were selected so that a pores was filled partially and a cylindrical void appeared in its center (Fig. 26). The as-prepared samples were investigated via DSC, and it was found that nanometer-scale spatial restrictions have the strongest effect on crystallization of the polymer. Figure 27 compares the DSC curves measured for crystallization and melting of the bulky PEO and PEO in the form of nanotubes with a wall thickness of ~100 nm. As is seen, the crystallization temperature of PEO decreases by ~50°C.

A similar behavior was observed during crystallization of nanotubes based on PVDF [170], syndiotactic PS [70, 167], PE [168], some block copolymers, etc, [158, 171].

In the most general terms, it may be stated that, during nanometer-scale spatial restrictions, crystallinity of the polymers decreases, the level of supercooling (the difference between equilibrium temperatures of melting and crystallization) increases, and the melting temperature declines with a decrease in the diameters of pores [168, 171].

The ratio between the rate of crystallization and the level of supercooling, ΔT, or crystallization temperature T_{cr} is usually used to discuss the mechanism of crystallization. In large pores ($D > 50$ nm), crystallization occurs at small ΔT and its rate noticeably depends on T_{cr}. In smaller pores ($D < 50$ nm), in contrast, crystallization occurs in a wider temperature interval ΔT and manifests a weaker dependence of the rate of crystallization on T_{cr} [171]. In accordance with the classical nucleation theory, a strong temperature dependence of the rate of crystallization in large pores provides clear evidence that crystallization via heterogeneous nucleation occurs.

An inspection of the above data makes it possible to conclude that, during the crystallization of polymers in the confined volume, the nucleation process prevails over the process of growth, and this situation strongly influences the structure and properties of the final product. It is evident that spatial restrictions primarily affect the process of polymer nucleation because the critical size of crystallization nucleus is usually several nanometers.

The crystallization of low-molecular-mass and high-molecular-mass compounds in the bulk almost always occurs via the heterogeneous mechanism. Heterogeneous nucleation is associated with the presence of any kind of random admixtures, particles of dust, etc. in the polymer melt. However, in principle, crystallization may be implemented via the homogenous mechanism. This possibility is easily implemented exactly in the case when crystallization is performed under conditions of spatial restrictions.

If the crystallizable polymer is divided into finer and finer independent fragments (domains), then inevitably the time will come when all heterogeneous nuclei occurring in it will not be present in all isolated domains into which the initial monolith was divided. As a result of dispersion, the initial crystallizable polymer turns out to crumbled into domains containing heterogeneous nuclei and lacking these nuclei (Fig. 28) [172].

Homogeneous nucleation in the lengthy polymer bulk occurs during density fluctuations; as a consequence, the preferred direction of crystallite growth is absent and, in narrow pores, the wall of a pore itself serves as a heterogeneous nucleus (Fig. 29) [173]. It is well seen that crystallization of the polymer in narrow pores is accompanied by the orientation of crystallites with respect to the pore axis. In the next section, the orientation effects accompanying crystallization of polymers will be considered in more detail. Note that nucleation observed in narrow pores looks heterogeneous, although, in this case, the level of supercooling is much higher than that usually observed in heterogeneous nucleation. At the same time, during heterogeneous nucleation, the level of supercooling is usually much smaller than that in homogeneous nucleation. A high level of supercooling during crystallization of the polymer in narrow pores is usually explained by the fact that, in addition to well-known and certain kinds of nucleation (heterogeneous and homogeneous), another kind of nucleation is observed in confined vol-

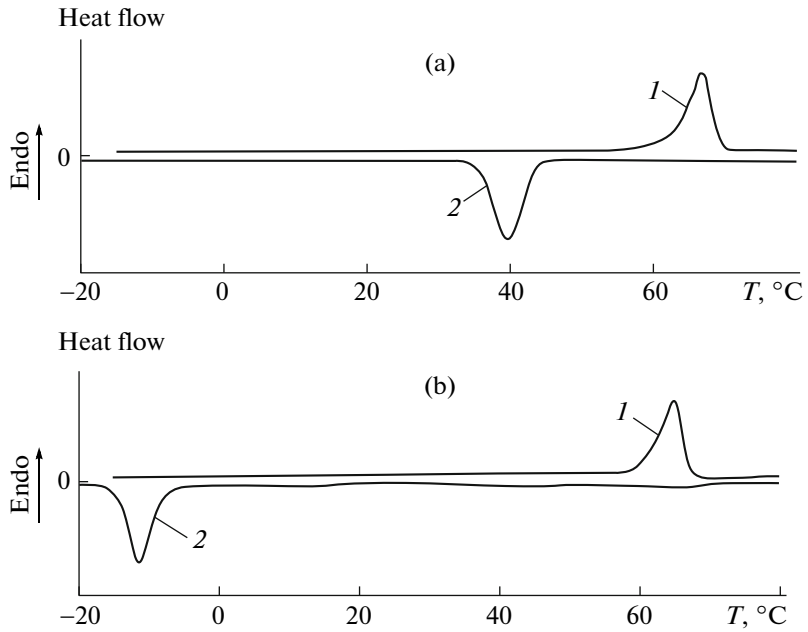

Fig. 27. DSC thermograms of (*1*) melting and (*2*) crystallization of PEO (a) in the bulky state and (b) in the nanotube with a wall thickness of ~100 nm [170].

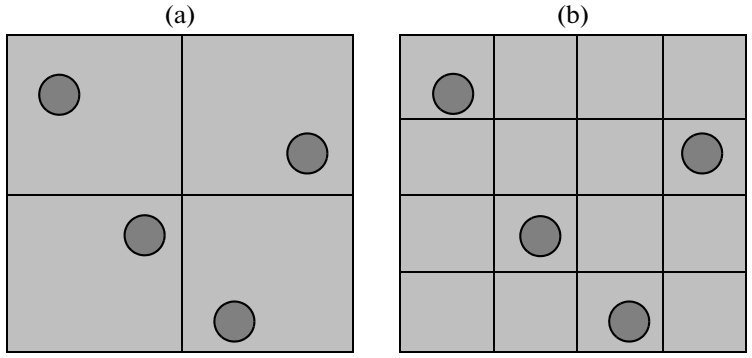

Fig. 28. Scheme illustrating division of the crystallizable polymer into individual domains (black circles) of nanometer sizes. (a) The sizes of domains are high, so that each of them contains at least one heterogeneous nucleus of crystallization (crystallization occurs via the mechanism of heterogeneous nucleation); (b) the amount of individual isolated domains doubled, and now a part of the domains lacks heterogeneous nuclei (crystallization occurs via the heterogeneous mechanism in domains containing nuclei and via the homogenous mechanism in domains free of nuclei) [172].

umes. This nucleation is referred to as surface nucleation. In fact, this is heterogeneous nucleation, but it occurs not on alien inclusions in a polymer melt (solution) but on the walls of nanopores and crystallization occurs at higher temperatures than homogeneous nucleation does. When the volume-to-diameter ratio of the polymer is small, this type of nucleation becomes very substantial.

The effect of the size (diameter) of the PVDF nanorod prepared in the AOP-based template on the thermal behavior of PVDF was studied [174]. The DSC data confirm that homogeneous nucleation insignificantly contributes to crystallization of the ensemble of individual PVDF tubes with diameters of 400 nm, whereas nucleation solely occurs if the diameters decrease to 35 nm (Fig. 30). It is well seen that a high level of supercooling during crystallization, which is typical for homogeneous nucleation, is observed during crystallization of PVDF for 35-nm-dia samples solely. At the same time, crystallization of the samples with diameters of 400 nm occurs practically in the same manner as that in the bulky polymer.

In [171], the kinetics of crystallization of linear PE inside AOPs was studied and it was inferred that, within pores with diameters less than 50 nm, the heterogeneous nucleation on the walls of pores domi-

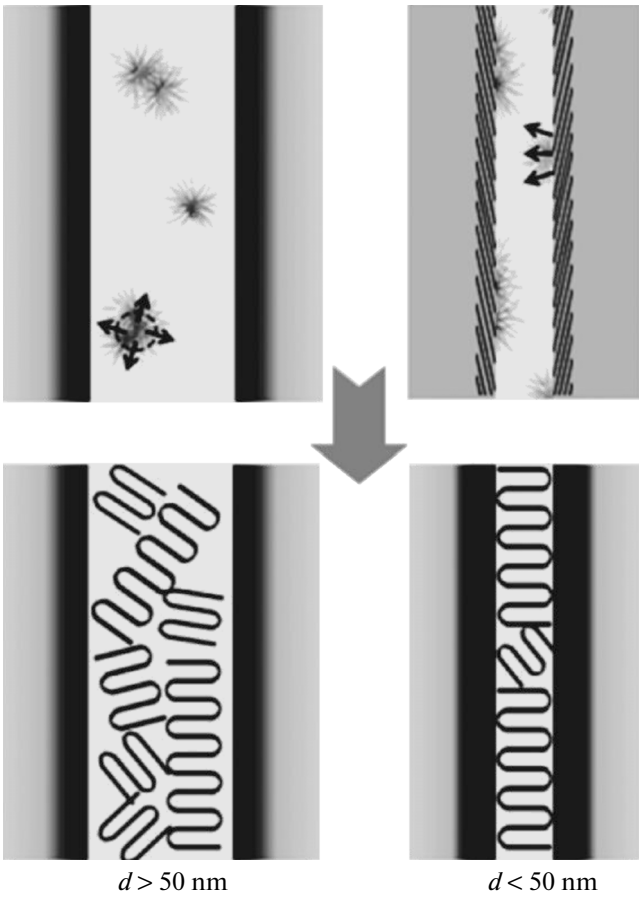

Fig. 29. Schematic representation of nucleation and crystallization of the polymer in wide (above 50 nm) and narrow (below 50 nm) pores [173].

nates, whereas at pore diameters of 62 and 110 nm, crystallization is mostly initiated by the homogeneous formation of nuclei. Exponent n in the Avrami equation, which depends on the geometry of crystal growth and the mechanism of nucleation, is smaller in value in the case of PE crystallization in nanopores than that in the bulk. This fact indicates that the growth of crystals in pores is hampered and that nucleation occurring at higher levels of supercooling dominates.

Now let us briefly touch upon the issue of orientation of crystals in the confined volume of rigid templates. As a rule, the c axes of chains directed normally to the plane of lamellas (Fig. 9) are aligned perpendicularly to the axes of pores of rigid templates, as determined by the growth of crystals along the pore axes. Although the studies devoted to this problem are scarce [167, 168, 170, 171, 174], it is clear that crystallization in narrow pores of rigid templates may depend on the presence or absence of the reservoir of the bulky polymer in contact with the polymer within the pore (Fig. 31).

The authors of [70, 175–176] inferred that crystallization in nanorods prepared via soaking with a polymer (syndiotactic PS) melt is controlled by three types of nucleation and subsequent growth. The first type consists of the same heterogeneous nuclei as in the bulk, but their amount is very small, as evidenced by a small amount of spherulites and their large sizes. The second type of nuclei appears on the walls of nanopores. When the melt enters into the nanopore under the action of capillary forces, the polymer chains extend. The resulting longitudinal flow stimulates the spatial orientation of chains along the nanopore axis [176, 177]. Thus, the extended chain segments facilitates the formation of nuclei with c axes parallel to the walls of nanopores [176]. Nuclei may then develop into crystallites with a parallel or close-to-parallel orientation of the c axes.

The third type of nucleus is formed in the bulk, which plays the key role in the orientation of crystallites in the nanopore. In the above experiments, the nanorod was linked with the bulk of the same thermal prehistory. This situation presumes that crystallites formed in the bulk may grow into the nanopore and may serve as nuclei for polymer crystallization [174, 176].

Crazing of Polymers in Liquid Media

Let us briefly consider another type of two-dimensional spatial restrictions under which the crystallization of polymers may be implemented. The case in point is one of the fundamental properties of glassy and crystalline polymers: their crazing ability. Remember that, in fact, crazing of a polymer is its dispersion into aggregates of oriented chains having diameters of several nanometers [178–180] (Fig. 32).

The structure shown in Fig. 32 spontaneously appears during stretching of polymers in active liquid media. It is important that the diameters of interconnected pores in this structure are tens of nanometers. The possibility of development of the given structure is associated, in particular, with its continuous filling with the surrounding liquid. In other words, crazing is not only a method for the development of a unique fibrillar–porous structure but also a method for delivering any component of another chemical type into it [180].

The introduction of crystallizable low-molecular-mass compounds into the nanoporous structure of crazes was studied in detail. It was shown that the crystallization of these compounds is accompanied by a well-defined orientation in asymmetric nanosized pores of crazes (Fig. 33).

Regardless of the chemical structure of the polymer and the type of introduced crystallizable low-molecular-mass compound, in all cases, it crystallizes to give rise to highly ordered textures. Figures 33a and 33b illustrate this phenomenon for PET containing low-molecular-mass compounds of various types [181]. It is clear that, in all cases, highly ordered textures are

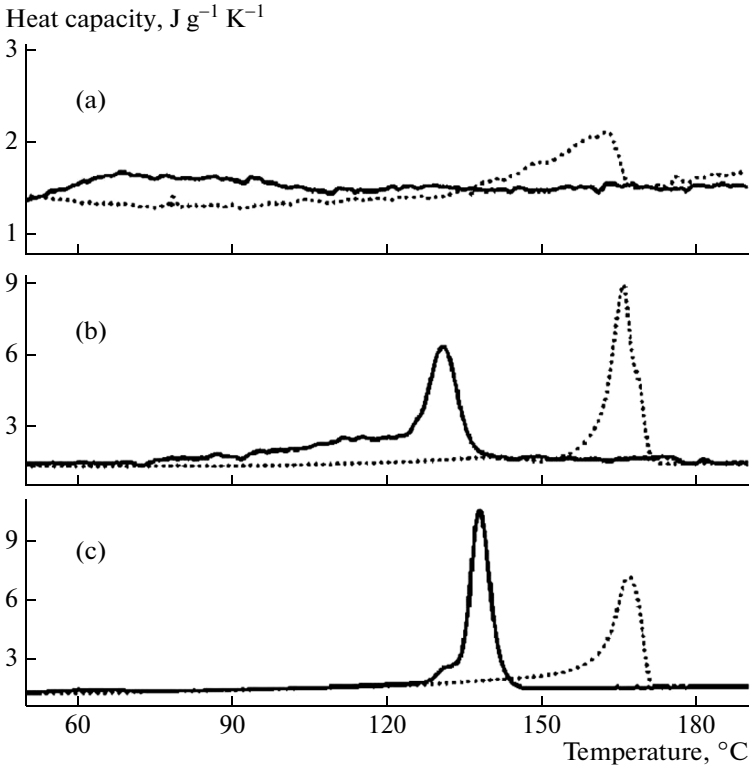

Fig. 30. DSC thermograms of PVDF: broken curves refer to heating, and solid curves refer to cooling: (a) the nanorod with a diameter of 35 nm, (b) the nanotube with a diameter of 400 nm, and (c) bulky PVDF [174].

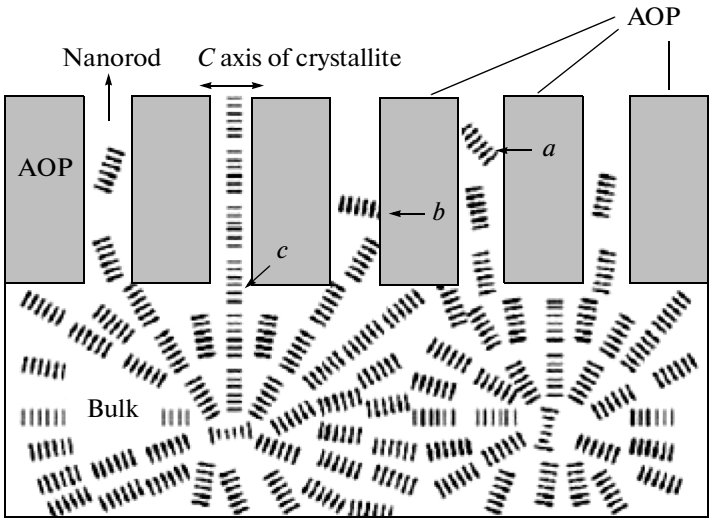

Fig. 31. Schematic representation of the development of isotactic PS crystallites in the nanopores of template based on oxide aluminum plates. Three types of nuclei contribute to the crystallization of the polymer in nanopores: (*a*) the random heterogeneous nucleus contained in the initial polymer, (*b*) the nucleus arising on the inner surface of the nanopore, and (*c*) the nucleus that has a structural relation (preserves the orientation of crystallites in the spherulite) to the crystalline structure of the bulky polymer and is inherited by the crystallizable polymer in the nanopore [175].

formed and their X-ray diffraction patterns are similar to X-ray diffraction patterns of single crystals.

The considered phenomenon is of a general pattern and is observed when crazed crystallizable polymers (PET, PC) and amorphous polymers (atactic PMMA) are used as matrixes [182, 183]. All described features are preserved after the introduction of both ionic and molecular crystals into crazed polymer matrixes.

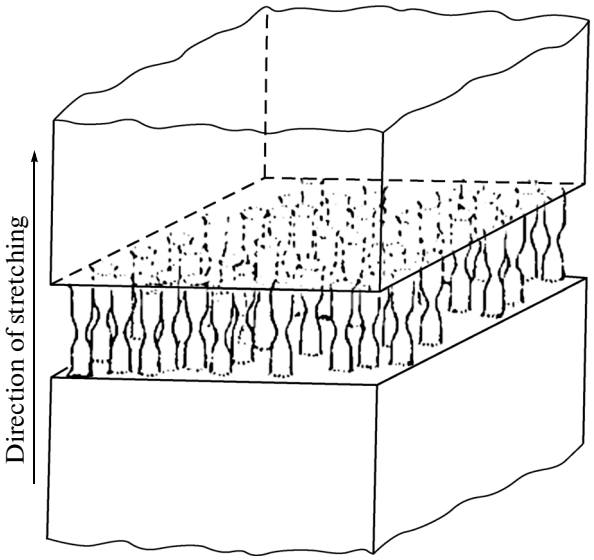

Fig. 32. Schematic representation of the craze structure [179].

It is important that, in recent years, successful attempts have been made to introduce high-molecular-mass compounds into nanoporous structures of crazes. The methods of this introduction were described in detail in [184–186], and, here, we would like to cite the initial data on the structural studies of such polymer–polymer composites.

In [187], the second crystallizable polymer (PEO with $M = 2 \times 10^4$) was introduced into crazed polymer matrixes (PP). This procedure was performed directly during the crazing of PP in the course of its stretching in PEO solutions. The content of the introduced PEO after solvent removal was 45 wt %. The resulting composites were investigated via FTIR spectroscopy and X-ray diffraction. It was found that poly(ethylene oxide) introduced into the PP crazes crystallizes in the same manner as low-molecular-mass compounds introduced into crazes. Note that, like low-molecular-mass compounds, PEO crystallizes in PP pores to give rise to crystallites oriented in a certain manner. In Fig. 34, X-ray diffraction data are compared with the scheme of arrangement of PEO crystallites in the crazed matrix of PP.

As follows from Fig. 34, PEO crystallites are oriented normally to the axes of pores in the crazes of PP, that is, demonstrate the edge-on orientation lamella with respect to the substrate (in this case, to the surface of fibrills). This arrangement of crystallites with respect to the confined surface was observed at certain temperatures of PEO crystallization, for example, in nanolayers, block copolymers, and nanotubes [169, 188, 189].

Crystallization of Polymers in Microemulsions and Nanoemulsions

Let us consider the data about the specific features of polymer crystallization in microemulsions, nanoemulsions, and dispersions. Under these conditions, the growth of crystals is confined in all directions; hence, the effect of nanometer-scale spatial restrictions on the crystallization of polymers manifests itself most vividly.

At present, there are several techniques that make it possible to obtain the community of droplets (domains) having micron or nanometer sizes. Specifically, in [190], a blend of polymers (PEO and block copolymer of PEO with ethylene–butylene copolymer) was prepared from a common solvent. After mixing, a microemulsion was formed. It was treated with ultrasound, and the solvent was removed. The resulting emulsions contained nanoparticles of the crystallizable component (PEO) with sizes of 80–120 nm.

Generally, the method of phase separation in polymer blends is very popular and has found wide use for obtaining nanoemulsions (nanodispersions) in order to gain insight into the effect of spatial restrictions on the crystallization of polymers. In such a manner, composites containing nanosized domains of practically any crystallizable polymer were prepared. Published data are available about the crystallization of such polymers as isotactic PS [191–196], isotactic and

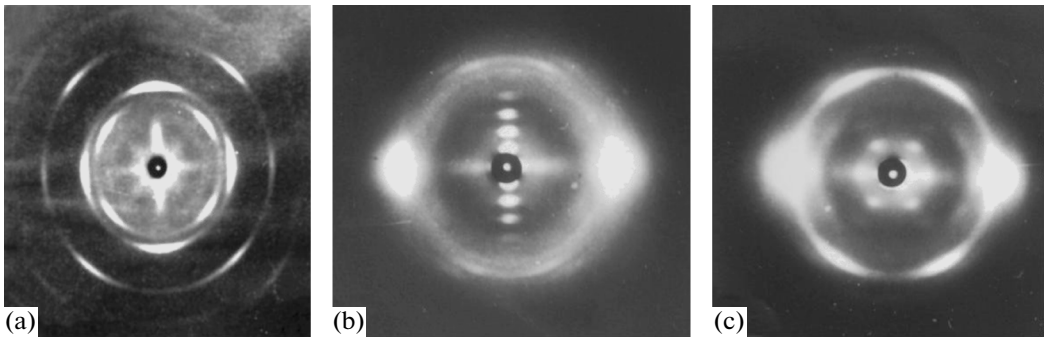

Fig. 33. X-ray patterns of (a, b) crazed PET samples containing (a) KI and (b) *n*-octadecane and (c) the crazed PC sample containing pentadecanoic acid. The axis of polymer stretching is vertical [181].

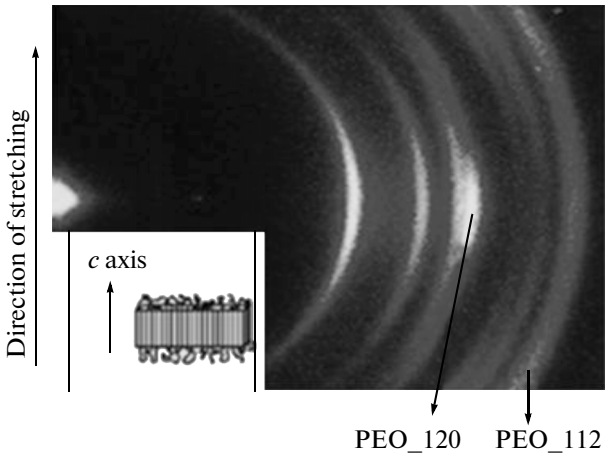

Fig. 34. Orientation of PEO in polypropylene-based nanocomposites prepared via the crazing technique. The axis of stretching is vertical [187].

syndiotactic PPs [197–199], PC [200, 201], PVDF [202], PET [203], poly(*L*-lactide) [204], and PMMA [205] during nanometer-scale spatial restrictions.

Methods of preparing nanodroplet dispersions based on PEO and PE were developed [172, 206–211]. To prepare dispersions, thin polymer films were deposited on a substrate and then annealed. Because of the decrease in the wetting ability (dewetting), small droplets appeared on the substrate in which crystallization was performed.

There is another possibility to form nanosized droplets of crystallizable polymers. Ultrathin fibers prepared via electrospinning are often used for this purpose. The diameters of fibers prepared via traditional spinning from polymer melts and solutions are up to several tens of microns and are primarily determined by the needs of the textile industry. In recent years, the interest in fiber formation via electrospinning has increased considerably because this method makes it possible to manufacture polymer fibers with diameters from several microns to several tens of nanometers [212–219].

Electrospinning differs substantially from the traditional method of producing polymer fibers because electrospinning relies on the use of electrostatic forces rather than mechanical stresses [220–222]. The fact that polymer fibers of such small diameters can be obtained is important because this phenomenon provides another approach to the study of the effect of nanosized droplet systems on the crystallization of polymers in them.

Finally, the method of preparing nanosized spherical particles (droplets) through the force assembly of polymer systems should be mentioned (see the chapter Crystallization of Polymers under Conditions of Nanometer-Scale Spatial Restrictions, under the section Multilayer Polymer Nanosystems). With the use

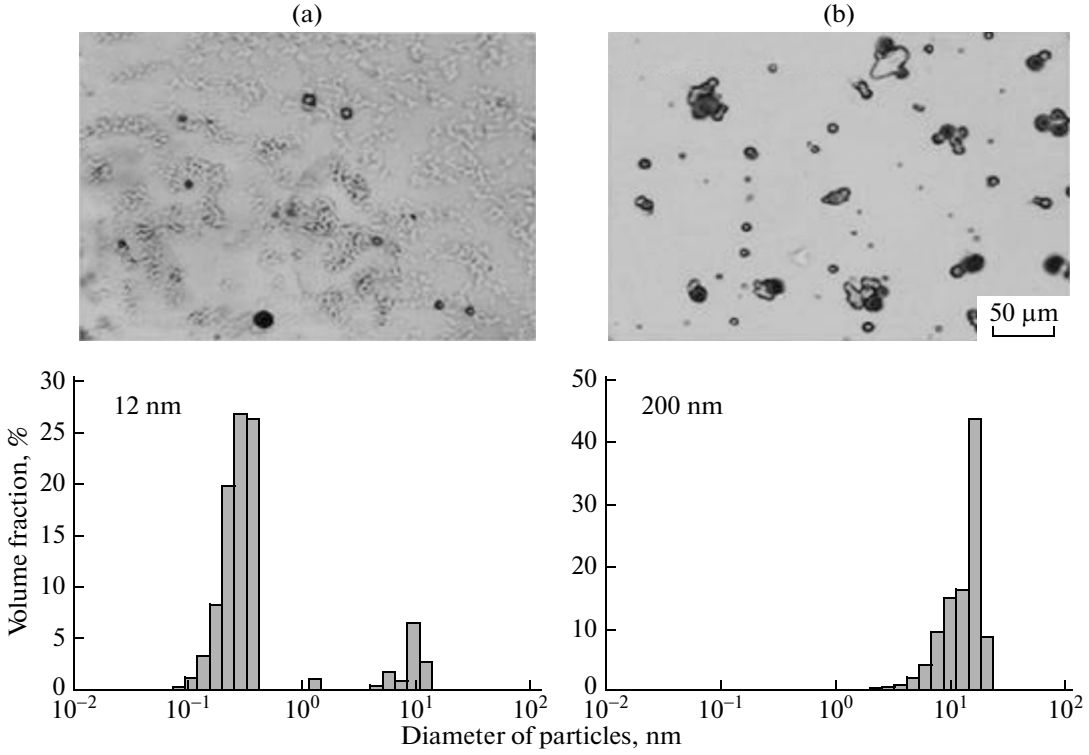

Fig. 35. (Upper panels) Optical micrographs of PP dispersions prepared during remelting of PS/PP multilayer films with thicknesses of PP layers of (a) 12 and (b) 200 nm and (lower panels) their corresponding size distributions [223].

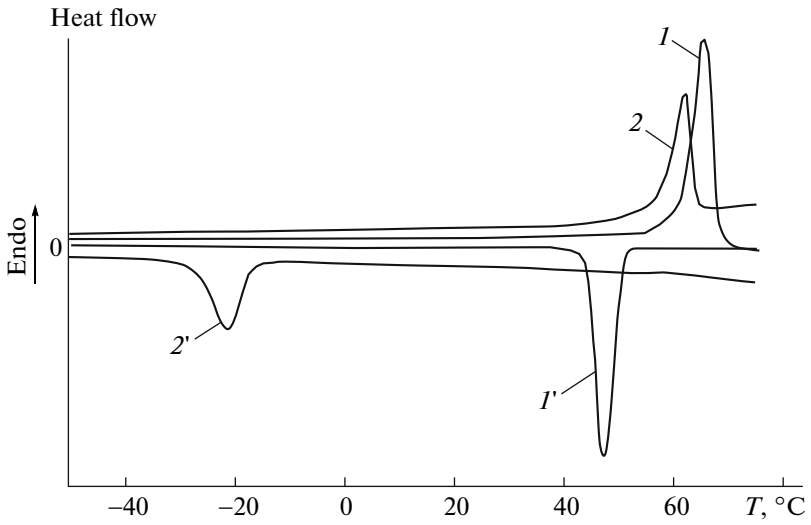

Fig. 36. DSC thermograms of PEO with $M = 4 \times 10^4$ in (*1, 1'*) the bulky state and (*2, 2'*) the microemulsion with a mean diameter of particles of 100 nm [190, 225, 226]: (*1*, *2*) heating and (*1'*, *2'*) cooling.

of this method, multilayer polymer systems with layers of almost any thickness (down to several nanometers) may be prepared. If the layers are built of immiscible polymers and one of them is crystallizable, annealing of this system leads to stratification accompanied by formation of a community of nanosized droplets.

Note that the mean sizes of spherical particles (droplets) in systems formed after annealing may be tailored through variation in the thicknesses of layers of the crystallizable component in the multilayer film (Fig. 35) [223]. Thus, there are several ways to create populations of nanosized droplets of crystallizable polymers. This circumstance opens a real chance to estimate the effect of geometric three-dimensional restrictions on the specific features of crystallization. The methods of obtaining polymer nanoemulsions (nanodispersions) were surveyed in length in [224].

Let us examine the most characteristic features of polymer crystallization in microemulsions and nanoemulsions. As is seen from Fig. 36, nanosized restrictions of the polymer in a miniemulsion exert the strongest effect on its crystallization [225–226]. For example, for PEO, the crystallization temperature decreases by 42.8°C relative to its value for the bulky polymer; as a result, its nanometer droplets turn out to be still liquid at room temperature.

Such a pronounced change in the behavior of the polymer during its crystallization under spatial confined conditions is of a general character. As was shown a long time ago [227–236], in small droplets, all substances crystallize at much lower temperatures than those in the bulk.

As was noted above, there are at least two types of nucleation during crystallization: homogeneous and heterogeneous. Crystallization usually proceeds during heterogeneous nucleation at small levels of supercooling. However, at huge levels of supercooling, homogeneous nucleation may be implemented, as was first shown in the study of crystallization in droplets [233, 234]. Crystallization under confined conditions shifts nucleation from heterogeneous to homogeneous. This is related to the fact that several active nuclei controlling crystallization in the bulk are now distributed in several droplets, while other droplets remain without any nuclei [228, 237]. As a result of this distribution of nuclei, the majority of the polymer crystallizes in droplets (microdomains) free of heterogeneous nuclei via the homogeneous mechanism. That is why such a strong depression of the crystallization temperature of the polymer in nanosized domains relative to that in the bulky polymer is observed.

This sharp transition from heterogeneous nucleation to homogeneous nucleation is a rare phenomenon. It occurs when the amount of microdomains (nanosized droplets or nanoparticles) in the dispersed polymer is immeasurably higher than the amount of heterogeneous nuclei present in the initial bulky polymer. Exactly this situation is shown in Fig. 28. As was mentioned above, the formation of nanosized domains easily occurs during phase separation of polymer blends when the amount of the dispersed phase is small [238]. Let us consider the thermodynamic behavior of such a system based on amorphous PS and a crystallizable component, isotactic PP [239]. Figure 37 presents the DSC thermograms of individual components (PS and isotactic PP) and their blend containing 20% of the crystallizable component (isotactic PP)

It is well seen that the thermogram of the polymer blend contains several crystallization peaks, but one of them (designated peak *A*) corresponds to crystallization of the bulky isotactic PP. The causes of the observed phenomenon are the specific features of

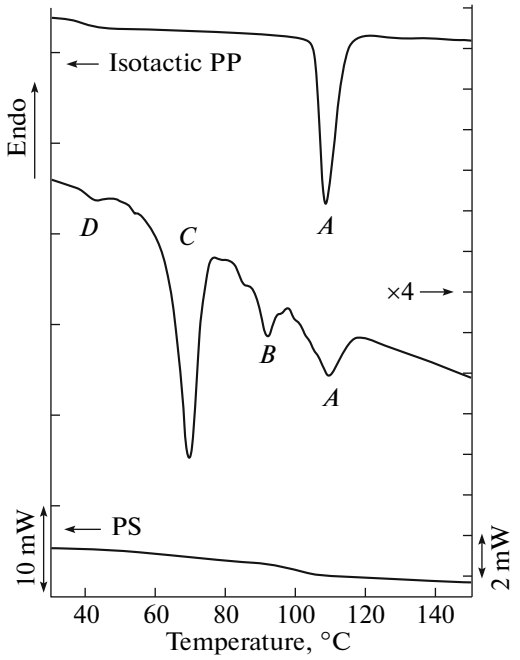

Fig. 37. DSC thermograms of isotactic PP, PS, and their blend with a component ratio of 80 : 20. *A* is the peak of crystallization of bulky isotactic PP [239].

crystallization of the polymer dispersed in microdomains. When PS is mixed with isotactic PP, the latter forms droplets with sizes of ~1 μm. The amount of these droplets (10^{11} L/cm^3) is much higher than the amount of nuclei in the bulk (9×10^6 L/cm^3), as evidenced by light microscopy [239]. Heterogeneities present in PP feature different efficiencies and are activated at different supercooling levels. In the bulk, only the most active heterogeneities are activated at small levels of supercooling and yield a single peak in Fig. 37. Less active heterogeneities cannot be activated under these conditions. As a consequence, DSC thermograms show several crystallization peaks, each of which corresponds to crystallization of the polymer on nuclei of various activities. It is evident that the most inactive nuclei that "trigger" at the highest levels of supercooling are responsible for the homogeneous mechanism of nucleation. As is seen in Fig. 37, crystallization peak *A* takes the same position as in the bulk and, hence, it may be attributed to crystallization in microdomains that contain the most active heterogeneities. Peaks *B* and *C* correspond to crystallization in droplets containing less active nuclei that are activated at high levels of supercooling. Finally, peak *D* corresponds to crystallization in pure microdomains that are free of heterogeneous nuclei and, therefore, crystallize at the highest degrees of supercooling. Because exotherm *D* is still above the glass-transition temperature of PP, it is unlikely that this crystallization is really homogeneous; most likely, this is the crystallization of droplets in which surface nucleation occurs.

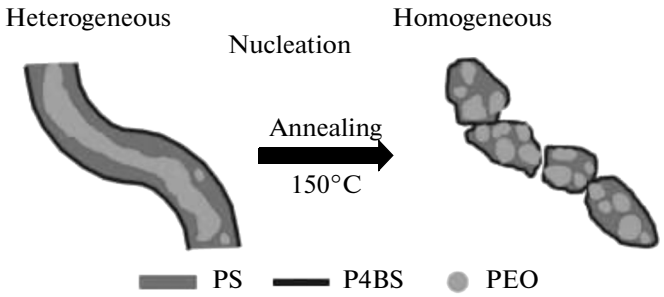

Fig. 38. Schematic representation of the formation of PEO nanosized droplets during annealing of the PS–PEO blend fiber covered with a poly(4-butyl styrene) (PBS) shell [241].

The multiplicity of crystallization peaks is related to the deficiency of active nuclei in every microdomain present in the blend. If heterogeneous nuclei are introduced into microdomains, then the multiplicity of peaks should disappear. The phenomenon of peak multiplicity during crystallization of the polymer under confined spatial conditions was referred to fractional crystallization. This term was coined in [240] to describe multiple crystallization exotherms observed in the DSC study of polymer blends, when the ensemble of microdroplets (microdomains) is cooled from melt, as opposed to a single crystallization peak observed in the bulk.

For fractioned crystallization to occur, the amount of droplets (microdomains) should be at least on the same order of magnitude as the amount of active heterogeneous nuclei in the bulky polymer. During mixing of the crystallizable polymer with the immiscible noncrystallizable matrix, droplets free of nuclei and droplets containing nuclei appear. The presence of several crystallization exotherms is explained by the fact that droplets including nuclei of different activities and droplets free of them crystallize (are activated) at different degrees of supercooling.

The appearance of fractional crystallization was very vividly demonstrated in [241], where the population of nanodroplets was created via annealing of blend fibers based on PEO and PS prepared via coaxial electrospinning [242] and having the core–shell structure (Fig. 38). After annealing at a temperature above 150°C, the fiber is dispersed into a system of aggregates containing nanosized inclusions of the crystallizable component (PEO).

DSC measurements give insight into crystallization processes of blend fibers annealed at different temperatures. As follows from Fig. 39, when the blend fiber is annealed at a temperature below the glass-transition temperature of PS (85 and 95°C), the main crystallization peak is observed at 40°C, while a small peaks is seen at −20°C. As was proposed in [206, 243], high-temperature and low-temperature processes are induced by heterogeneous nucleation and homogeneous nucleation, respectively. When annealing is per-

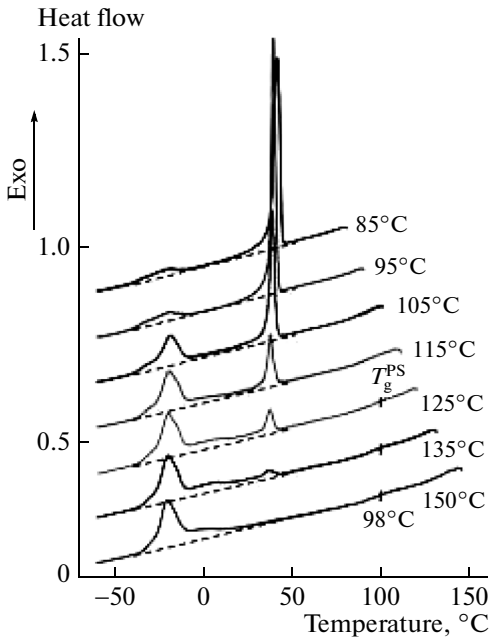

Fig. 39. DSC thermograms of PEO–PS blends prepared via annealing of ultrathin fibers obtained via electrospinning. The numbers next to the curves designate the annealing temperatures of blend fibers [241].

formed in the region of the glass-transition temperature of PS (e.g., at 105 and 115°C), the intensity of the low-temperature peak increases slightly, while the main heterogeneous peak remains almost the same. After a further increase in the annealing temperature (125–135°C), the main heterogeneous peak at 40°C begins to decrease gradually (its surface area is decreased), while the homogenous peak remains the same. A blurred broad peak between 40 and −20°C may be attributed to heterogeneous nucleation under confined crystallization [241]. When the blend was annealed at 150°C, many weak crystallization peaks appeared at −20, −2.5, and 12°C along with a heterogeneous peak at 40°C. This behavior is typical for fractional crystallization [241].

Block Copolymers

Block copolymers are unique multiphase systems in which immiscible components have as a rule the structure of regular superlattices. Depending on synthesis conditions, the morphology of block copolymers may be different (spheres, cylinders, lamellas, or more complex structures with double-phase continuity).

From the viewpoint of the subject matter of this review, two circumstances should be taken into account. First, the sizes of phase domains in block copolymers are a few nanometers, and, second, at least one of the blocks may be crystallizable. These circumstances make it possible to use block copolymers

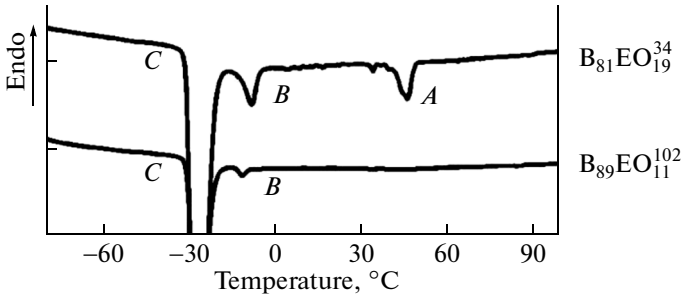

Fig. 40. DSC thermograms for crystallization of block copolymers $B_{81}EO_{19}^{34}$ and $B_{89}EO_{11}^{102}$ [245].

to study the effect of spatial restrictions on crystallization of a polymer if its molecular mobility is confined by chemical bonds with other immiscible components of the system.

Let us consider the crystallization of blocks of the crystallizable polymer PEO in the block copolymer PEO–PB [245]. In this case, the crystallizable PEO occurs in the environment of the rubberlike amorphous polymer PB, for which the glass-transition temperature is approximately −70°C. Two types of block copolymers were investigated, namely, $B_{81}EO_{19}^{34}$ and $B_{89}EO_{11}^{102}$, where the lower index corresponds to the composition of the block copolymer and the upper index corresponds to molecular mass of the PEO block.

Block copolymer $B_{89}EO_{11}^{105}$ had the morphology of spherical domains that were chaotically dispersed in the PB matrix, and $B_{81}EO_{19}^{34}$ had the mixed morphology of short cylinders and spheres with the spheres prevailing. In accordance with the structural data, the sizes of domains in $B_{81}EO_{19}^{34}$ were larger than those in $B_{89}EO_{11}^{105}$. In both cases, the sizes of spheres were consistent with the sizes of spheres typical for other systems [246–249].

Figure 40 presents DSC thermograms measured for crystallization of both block copolymers. Note that, as for other above-considered systems, fractional crystallization (crystallization occurs via several steps with well-resolved DSC peaks) is typical for block copolymers. This is expected because, for example, in the case of $B_{89}EO_{11}^{105}$ the amount of microdomains (transmission-microscopy data) is 10^{16} cm^{-3}, whereas the amount of highly active heterogeneities (nuclei) in PEO is 10^6 cm^{-3}. Hence, in the volume of the block copolymer, nucleation and, hence, crystallization of PEO blocks may occur at various degrees of supercooling.

In the case of $B_{81}EO_{19}^{34}$ having the mixed morphology consisting of spheres and cylinders, the PEO phase contains a small amount of microdomains free

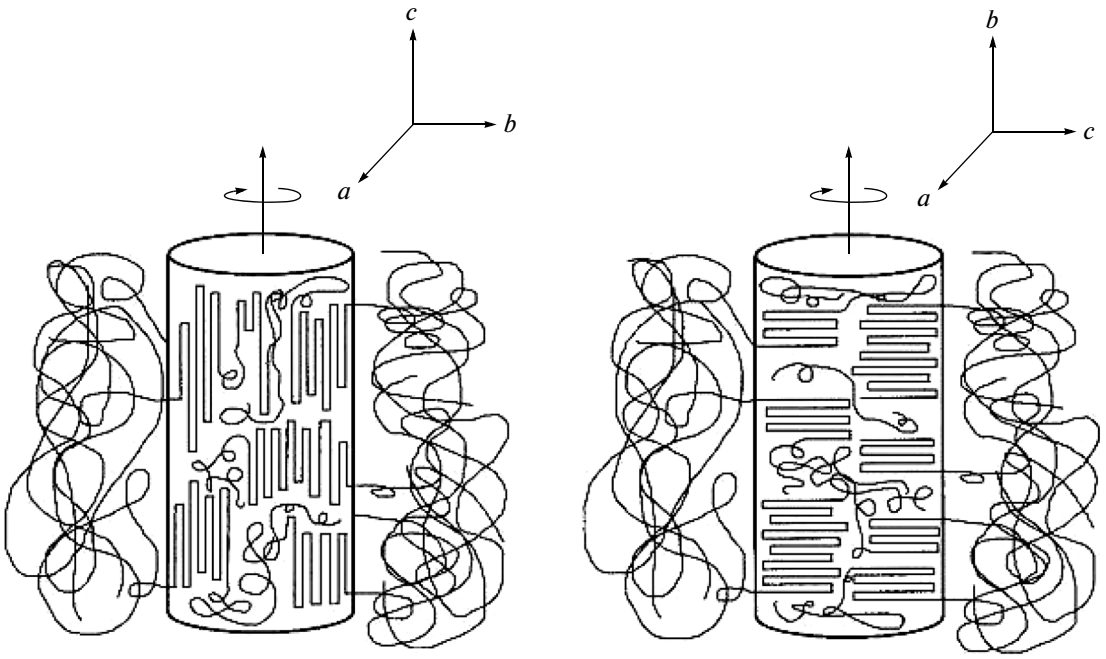

Fig. 41. Schematic representation of two possible orientations of chains in cylindrical domains of the block copolymer [252].

of heterogeneous nuclei; as a consequence, the small exotherm denoted *A* had the same crystallization peak as the individual PEO. Second peak *B* emerges during crystallization from the melt owing to crystallization of a group of microdomains containing less active heterogeneities.

Finally, peak *C* seen at the highest levels of supercooling may be related to the crystallization of microdomains free of heterogeneities. For both block copolymers, pure crystallization in heterogeneity-free domains dominates at high supercooling levels (–25°C). However, as was shown in [250, 251], PEO in the individual (homogeneous) state yields supercooling on the order of –45°C; therefore, it is assumed that supercooling of –25°C is related to the so-called surface crystallization or crystallization at the boundary with the PB block [245, 250, 251]. As was mentioned above, the interfacial surface frequently features a high nucleation activity that becomes especially pronounced for systems with large specific surfaces.

It should be emphasized that the literature devoted to structuring in block copolymers is very voluminous and we do not pretend to provide an exhaustive analysis. In the present review, we would like only to mention that crystallization under spatially confined conditions is among the characteristics features of these systems. In particular, orientation effects occurring during crystallization in other spatially confined polymers are likewise distinct in microdomains of block copolymers. For example, Fig. 41 illustrates feasible spatial orientations of crystallites in the domains of block copolymers having cylindrical morphologies [252]. It is important that, although many features of crystallization of polymers in the confined volume manifest themselves for block copolymers as well, these systems exhibit certain specific features inherent in block copolymers solely. These are above all the influence of the composition of the block copolymer, the morphology of the crystallizable block, and the character of the intermolecular interaction between blocks.

For example, in the case of the block copolymer composed of miscible blocks of polyamide 6–polycaprolactam (PA-6–PCL), the growth of crystallites of PCL blocks is confined by the crystalline lamellas of PA-6 that are formed at higher temperatures [253].

When block copolymers crystallize from solutions, the selective solubility of blocks plays an important role. If the insoluble block can crystallize, then crystallization occurs under confined conditions and T_m and T_{cr} are depressed [254, 255]. However, during crystallization from solutions, one more factor affecting crystallization arises, namely, the solvent.

In conclusion of this section, let us consider recent study [256], in which the crystallization of block copolymers was implemented in the nanoporous structure of AOPs. In this study, geometric spatial restrictions acting on the crystallizable polymer in the block copolymer were combined with spatial restrictions related to the nanosized structure of the AOP. Block copolymers based on PEO and PCL were studied. Let us examine the data available only on one block copolymer PEO_{114}-*block*-PCL_{88}, where the digits denote the degree of polymerization for each block.

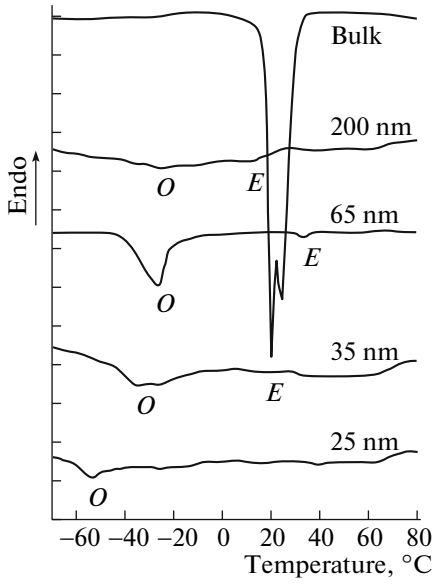

Fig. 42. DSC thermograms for crystallization of the PEO_{114}-*block*-PCL_{88} block copolymer in the bulky state and in the cylindrical nanopores of the AOP template. The numbers next to the curves refer to the diameters of cylindrical nanopores. Letters *O* and *E* designate homogeneous and heterogeneous nucleations, respectively [256].

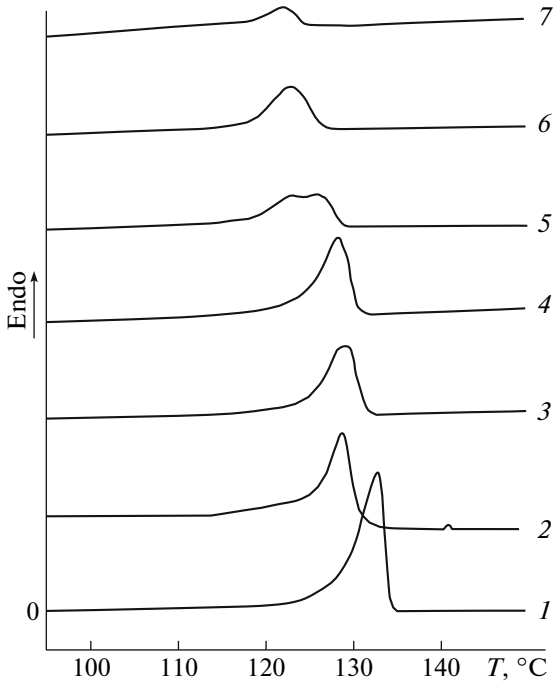

Fig. 43. DSC thermograms of (*1*) bulky PE, (*2*) the commercial product with crystallite diameters of 220 nm, and (*3*–*7*) PE crystallized in cylindrical pores with diameters of (*3*) 110, (*4*) 62, (*5*) 30, (*6*) 20, and (*7*) 15 nm [169].

It is significant that, in this block copolymer, both immiscible components are capable of crystallization; therefore, these block copolymers were studied in length [257–259]. It was shown that, in the bulk (a bulk sample) the block copolymer exhibits two crystallization peaks, at 25 and 20°C, which are related to the fractional crystallization of PCL [256]. The introduction of the block copolymer PEO_{114}-*block*-PCL_{88} into the nanosized cylindrical pores of the AOP-based template drastically changes the picture of its crystallization. As is clear from Fig. 42, the main crystallization peak shifts to a temperature of −26°C in 65-nm-dia nanopores and to a temperature of −53°C in 25-nm-dia nanopores. On the basis of complex structural studies, the authors of [256] stated that, in the nanoporous structure of the AOP-based template, the crystallization of PEO blocks is fully suppressed, while the crystallization of PCL blocks occurs via homogeneous nucleation at high levels of supercooling. The causes of such a complicated thermodynamic behavior of block copolymers are presently still unclear.

Effect of Crystallite Sizes on the Melting Temperatures and Heats of Melting of Polymers

As was noted above, during crystallization of a polymer in nanopores, the stage of nucleation prevails over the stage of crystallite growth. This circumstance inevitably entails formation of a product with very small crystallites. In turn, the decrease in the sizes of crystals is accompanied by an increase in the interfacial surface. As a result, the melting temperature declines.

The Gibbs–Thomson equation is commonly used to describe the dependences of T_m on the sizes of crystallites and interfacial surface energy [7, 260, 261]. It may be written as

$$\Delta T_m = T_m^\circ - T_m = 4\sigma\, T_m^\circ/(d\Delta H_m^\circ \rho_c), \qquad (1)$$

where T_m° is the equilibrium melting temperature of a crystal with infinite sizes, ρ_c is the density of the crystal, ΔH_m° is the specific heat of melting, and d is the diameter of a crystallite.

In the considered case of melting in the confined space, d is the diameter of a nanopore in which the polymer was crystallized. As follows from Eq. (1), melting temperature depression ΔT_m is inversely proportional to the diameters of pores.

Figure 43 shows the DSC thermograms of PE melting in narrow cylindrical pores of various diameters [168]. It is seen that, as the diameters of pores decrease, the melting temperature of PE declines appreciably.

In summary of this section, note that the heat of polymer melting depends on its spatial restrictions as well. This dependence reflects, in particular, the effect of the diameters of the pores in which crystallization of the polymer is performed on its degree of crystallinity. The decline in the degree of crystallinity of the poly-

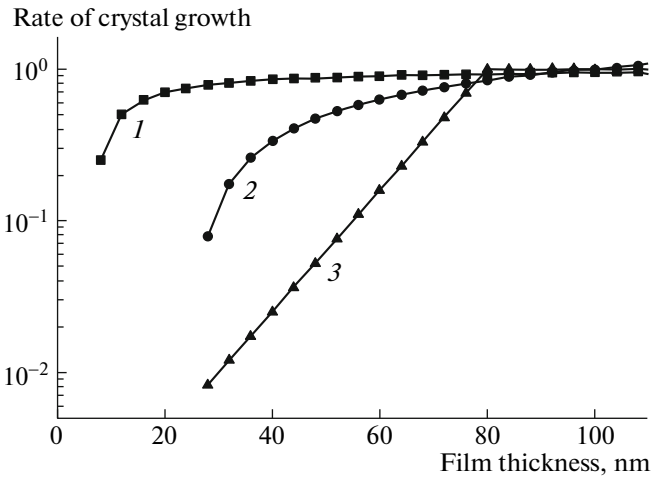

Fig. 44. Rate of crystal growth vs. film thickness for (*1*) isotactic PS [261] and (*2, 3*) PEO with M = (*2*) 272 × 10^3 [262] and (*3*) 10^5 [263].

mer under spatial restrictions may be very substantial. For example, as was shown in [168], the degree of crystallinity of PE in pores with diameters of 15 nm is as low as 30% (Fig. 25), while in the bulky state, the degree of crystallinity of PE is 71%.

Kinetics of Polymer Crystallization under Spatial Nanorestrictions

To this point, the effect of spatial restrictions on the structures and thermodynamic behavior of crystallizable polymers was discussed. It is evident that spatial restrictions exert a strong effect on the kinetics of crystallization of polymers as well.

As a rule, as the film thickness of the crystallizable polymer is decreased, the rate of its crystallization declines. Figure 44 plots the rates of crystal growth in thin polymer films reduced to the rate of crystallization of the bulky polymer [262–264]. It is well seen that the rate of crystal growth begins to decline considerably with a decrease in the thickness of the crystallizable polymer film (at a thickness of ~50 nm). This decline may be very considerable (by orders of magnitude), and in some cases, the rate of crystallization declines to almost zero. For example, as the thickness of the PEO film is decreased to several nanometers, the rate of its crystallization may be less than 1% of the rate of crystallization of the bulky polymer [265].

This decline in the rate of crystallization in thin (nanometer) layers turns out to be of a general pattern. As was mentioned above, under conditions of confined volume, the degree of crystallinity of the polymer and the rate of its crystallization decrease substantially [130, 265–272].

A question arises about the causes of such a strong reduction in the rate of crystallization in thin films of crystallizable polymers. In [273], the crystallization of PEO adsorbed in the form of a monolayer on a silicon surface was studied. During crystallization of this system, crystallization of the adsorbed polymer layer begins. Structural rearrangements accompanying crystallization are presented in Fig. 45. Crystallization is initiated on a certain heterogeneous nucleus and occurs via attachment of macromolecules situated vertically to form the lamellar structure (the flat-on orientation of the lamella relative to the substrate). After attachment of molecules to the crystal, the energy of crystallization is evidently released. The energy is higher if molecules are situated vertically, because, in this case, they have a greater amount of neighbors. The transport of molecules to the site of crystallization is the critical stage of this process. As in many other systems, this stage is limited by diffusion [274]. A change in the structure of the adsorbed polymer layer from the chaotic arrangement of macromolecules in the adsorbed layer to the vertical orientation of chains leads to depletion of the zone before the crystallization front. This process creates a free or empty zone on the surface because the surface area occupied by adsorbed molecules is higher than the surface area occupied by vertically crystallized chains. For a molecule to attach to the crystal, it should diffuse through the empty zone. Naturally, this kind of diffusion limits and sharply decreases the rate of crystallization on the whole.

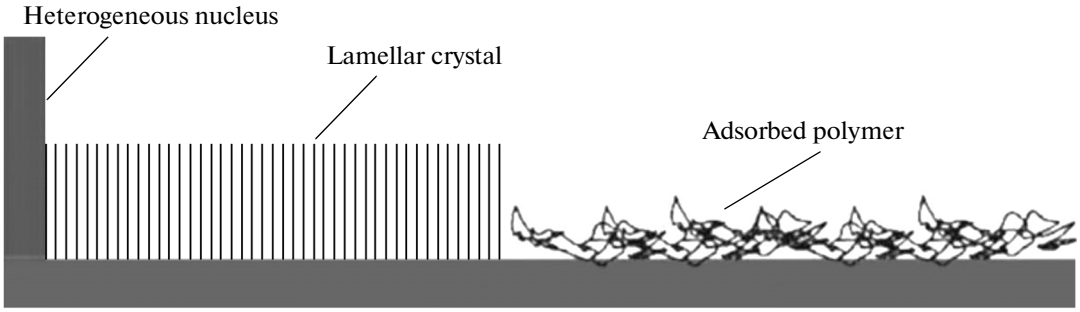

Fig. 45. Schematic representation of structural rearrangements accompanying the growth of lamellar crystals from the thin adsorbed polymer layer [273].

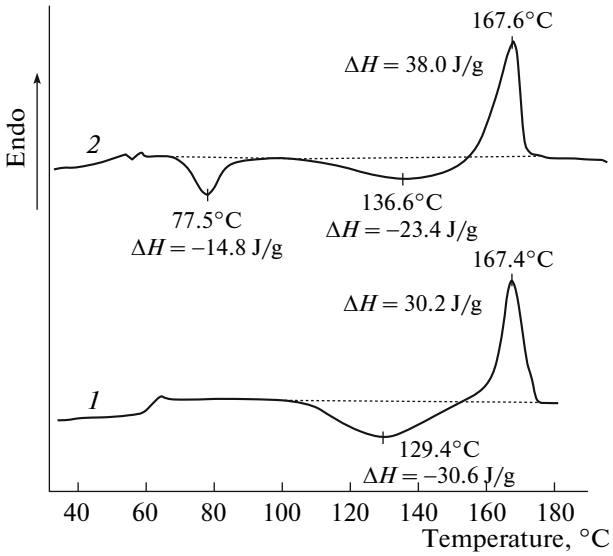

Fig. 46. DSC thermograms of (*1*) individual (monolithic) poly(*L*-lactide) and (*2*) poly(*L*-lactide) lyophilized from its 0.07% solution in dioxane [204].

This explanation of deceleration of the crystallization rate in thin polymer layers is not the only. Note that, in thin layers of the polymer, its T_g may change appreciably as well. In cases when there is an intense intermolecular interaction between the crystallizable polymer and the substrate, T_g of the polymer may increase noticeably (Fig. 5). A gain in T_g of the polymer at the interfacial boundary implies that its molecular mobility declines abruptly. At the same time, the rate of crystallization is determined in particular by the capability of macromolecules for structural rearrangements necessary for the development of crystal order. As a result, the given deceleration of the molecular mobility may cause a sharp decline in the rate of crystallization of the polymer in thin layers [275]. For example, the grass-transition temperature of PEO on a silicon wafer increases by more than 30°C in thin nanometer layers [265]. According to the authors of [265], this circumstance is responsible for a sharp decline in the rate of PEO crystallization.

The kinetics of crystallization in thin polymer layers was examined in many publications, and the data were treated in terms of the Avrami equation [276–278]. The main feature of this analysis is the well-defined reduction of index n in the Avrami equation relative to its value for the bulky polymer. For example, the kinetics of crystallization of the block copolymer containing PE blocks and the styrene–ethylene–butene copolymer was studied [279]. In this block copolymer, the crystallizable block (PE) is present in the form of spherical domains with diameters of 25 nm. For individual PE, $n = 2.4$ at 95°C, whereas for the block copolymer, $n = 1$. In this case, crystallization in the block copolymer occurs via the homogeneous nucleation. This first-order kinetics is typical for the crystallization of the polymer confined in the microdomain. This situation is expected because the three-dimensional free growth of crystals under nanometer restrictions is hampered.

Lyophilization Technique

An important point is that the above-described decline in the rate of crystallization of polymers was observed during crystallization of thin polymer films in contact with various kinds of substrates. At the same time, there is a universal way of creating nanometer-scale restrictions in polymers not in contact with substrates. This opportunity is provided by the lyophilization technique. In this case, the polymer solution is cooled with liquid nitrogen and then dry sublimation of the solvent is performed in vacuum. As a result, a highly dispersed polymer system is formed. It consists of isolated solid elements with sizes depending on the concentration of the initial solution. It was proposed [280] that the structures of such aerogels inherit to a certain extent the structure of the solution subjected to lyophilization. The microscopic study makes it possible to see that the aerogel consists of fibrillar-like elements with nanoscale diameters [281].

For these systems, as for other nanosized polymer phases, the values of T_g decrease [282–286]. It is very important that the lyophilization technique provides a way to study the effect of nanometer-scale spatial restrictions on the crystallization of polymers when the crystallizable polymer is not in contact with any substrate. This circumstance drastically changes the crystallization kinetics of the polymer under confined conditions. For example, PC, which poorly crystallizes in the bulky state, crystallizes intensely and very rapidly when it is lyophilized from dilute solutions [200]. The crystallization of polymers obtained via lyophilization of their solutions was studied in detail for such crystallizable polymers as isotactic PS [192–196], isotactic and syndiotactic PPs [198, 199], PC [201], PVDF [202], and PET [203]. In all cases, crystallization of the polymer accelerated abruptly relative to its crystallization in the bulk.

It appears that dispersion of the polymer via lyophilization sharply increases molecular mobility of the polymer; accordingly, its cold crystallization is affected as well. In [204], this phenomenon was revealed in the study of crystallization of poly(*L*-lactide). Figure 46 shows the DSC thermograms of the bulky poly(*L*-lactide) and poly(*L*-lactide) lyophilized from its 0.07% solution in dioxane.

As is seen from Fig. 46, spatial restrictions introduced into the polymer via lyophilization likewise affect the process of cold crystallization of the polymer. On the one hand, the peak of crystallization for the lyophilized sample (curve *2*, Fig. 46) shifts from 129 to 136°C and, on the other hand, a well-defined peak of cold crystallization appears in the low-temperature range (77°C). The glass-transition temperature,

which is usually observed for poly(*L*-lactide) at 60°C (Fig. 46, curve *1*), is absent for the sample lyophilized from a 0.07% polymer solution in dioxane (Fig. 46, curve *2*). It is assumed that a decrease in the temperature of cold crystallization is associated with a high molecular mobility of the polymer subjected to lyophilization. The same situation is responsible for T_g depression for poly(*L*-lactide) subjected to lyophilization.

An increase in the rate of crystallization for high-vacuum freeze-dried polymers is possibly associated with a marked depression of the glass-transition temperature of the polymer as a result of its dispersion (increase in molecular mobility) and with the absence of deceleration of polymer transport to crystallization sites during its diffusion over the substrate surface.

CONCLUSIONS

Our analysis of the literature data suggests that the dispersion of polymers into nanosized aggregates drastically affects the phase transitions and the ability of polymers to crystallize. At present, there are many systems in which the structuring of polymers is restricted at the nanolevel at least in one direction. These are thin polymer films or layers; polymers incorporated into nanoporous materials with various pore morphologies; blends and block copolymers; polymers whose structures are formed via lyophilization; and nanodroplets, nanofibers, nanotubes, nanocomposites, and many other more complex systems, including systems of the biological origin. For these systems, some general features of their structuring may be distinguished. Key factors determining the specific features of polymer structuring in the confined nanovolume are the size and morphology of the confined nanovolume and the conformation of the polymer in the surface layer, the level of its interaction with the surface, and the rate at which macromolecules can diffuse to the boundary of the growing crystal. At the same time, the above systems are characterized by their specific features, as manifested by the appearance of additional factors influencing structuring processes. For example, the nucleation and crystallization of polymers in nanopores depend on whether these processes occur independently in a pore or in contact with the surrounding polymer solution or melt. For block copolymers, along with common factors, the degree of connectivity of blocks set by their molecular masses plays a marked role. The structural diversity of block copolymers makes it possible to study the effect of one-dimensional and two-dimensional restrictions on crystallization in lamellar and cylindrical microdomains, respectively.

In the case of amorphous polymers, dispersion into nanometer sizes may decrease the glass-transition temperature by many tens of degrees. However, the contact of nanometer polymer aggregates with the substrate may decrease, not change, or even increase the glass-transition temperature of the polymer, depending on the character of its interaction with the substrate material. Spatial restrictions likewise affect the parameters of phase transitions of crystallizable polymers, thereby leading to a decline in the temperatures of crystallization and melting. As the sizes of restrictions are decreased, the heats of melting drop and the degrees of crystallinity of polymers decrease. Grinding of a polymer to nanometer sizes shows a strong effect on the type of nucleation during crystallization of the polymer. From the heterogeneous character of nucleation, which is usually observed during crystallization of bulky polymers, as the length of the polymer phase is decreased, the transition to the homogeneous character of nucleation occurs through the stage of fractional crystallization or heterogeneous surface nucleation on the walls of pores or on the surface of the solid substrate. The crystallization of polymers under confined conditions is accompanied by the orientation of crystallites in the nanometer asymmetric space and is determined not only by the size and morphology of restrictions but also by the character of its interaction with the solid surface and the ratio of the rates of nucleation and growth of crystals. The effect of restrictions on the crystallization of polymers may also lead to a change in the morphology of crystals.

The dispersion of polymers into nanometer domains is additionally reflected in the kinetics of crystallization of polymers. When the polymer is in contact with the rigid substrate, the rate of crystallization of the polymer decreases abruptly relative to the rate of its crystallization in the bulk, and, conversely, when the dispersed polymer is not in contact with the substrate (aerogels), the rate of its crystallization in nanometer domains increases sharply.

ACKNOWLEDGMENTS

This work was supported by the Russian Foundation for Basic Research (project nos. 15-03-03430a and 14-03-00617) and the Grant of the President of the Russian Federation for State Support of Leading Scientific Schools (NSh-1683.2014.3).

REFERENCES

1. R. A. Andrievskii, Ross. Khim. Zh. **46** (5), 50 (2002).
2. I. V. Melikhov, Ross. Khim. Zh. **46** (5), 7 (2002).
3. C. P. Poole and F. J. Owens, *Introduction to Nanotechnology* (Wiley, Hoboken; New York, 2003).
4. I. P. Suzdalev, *Nanotechnology. Physics and Chemistry of Nanoclusters, Nanostructures, and Nanomaterials* (KomKniga, Moscow, 2006) [in Russian].
5. N. G. Rambidi and A. V. Berezkin, *Physical and Chemical Foundations of Nanotechnology* (Fizmatlit, Moscow, 2009) [in Russian].

6. A. G. Kolmakov, S. M. Barinov, and M. I. Alymov, *Foundations of Technology and Application of Nanomaterials* (Fizmatlit, Moscow, 2013) [in Russian].
7. C. L. Jackson and G. B. McKenna, J. Chem .Phys. **93** (12), 9002 (1990).
8. A. I. Kitaigorodskii, *Molecular Crystals* (Nauka, Moscow, 1971) [in Russian].
9. M. Alcoutlabi and G. B. McKenna, J. Phys.: Condens. Matter **17** (15), R461 (2005).
10. *Polymer Nanocomposites*, Ed. by Y.-W. Mai and Z.-Z. Yu (Woodhead Publ., Cambridge, 2006).
11. A. D. Pomogailo, A. S. Rozenberg, and I. E. Uflyand, *Metal Nanoparticles in Polymers* (Khimiya, Moscow, 2000) [in Russian].
12. A. L. Volynskii and N. F. Bakeev, Polym. Sci., Ser. C **53** (1), 35 (2011).
13. A. L. Volynskii, A. Y. Yarysheva, E. G. Rukhlya, L. M. Yarysheva, N. F. Bakeev, Russ. Chem. Rev. **83** (11), 1003 (2014).
14. S. S. Ivanchev and A. N. Ozerin, Polym. Sci., Ser. B **48** (7–8), 213 (2006).
15. L. M. Bronstein, S. N. Sidorov, and P. M. Valetsky, Russ. Chem. Rev. **73** (5), 541 (2004).
16. C. R. Martin, Acc. Chem. Res. **28**, 61 (1995).
17. J. Jang, Adv. Polym. Sci. **199**, 189 (2006).
18. A. Arinstein and E. Zussman, J. Polym. Sci., Polym. Phys. Ed. **49**, 691 (2011).
19. D. Liang, B. S. Hsiao, and B. Chu, Adv. Drug Delivery Rev. **59**, 1392 (2007).
20. C. P. Barnes, S. A. Sell, E. D. Boland, D. G. Simpson, G. L. Bowlin, Adv. Drug Delivery Rev. **59**, 1413 (2007).
21. J. Martin, J. Maiz, J. Sacristan, and C. Mijangos, Polymer **53**, 1149 (2012).
22. G. B. McKenna, Eur. Phys. J.: Spec. Top. **189**, 285 (2010).
23. V. G. Rostiashvili, V. I. Irzhak, and B. A. Rozenberg, *Glass Transitions in Polymers* (Khimiya, Leningrad, 1987).
24. J. A. Forrest, K. Dalnoki-Veress, J. R. Stevens, and J. R. Dutcher, Phys. Rev. Lett. **77**, 2002 (1996).
25. J. A. Forrest and K. Dalnoki-Veress, Adv. Colloid Interface Sci. **94** (1–3), 167 (2001).
26. J. A. Forrest, K. Dalnoki-Veress, and J. R. Dutcher, Phys. Rev. E: Stat., Nonlinear, Soft Matter Phys. **56**, 5705 (1997).
27. M. D. Ediger and J. A. Forrest, Macromolecules **47** (2), 471 (2014).
28. C. M. Stafford, S. Guo, C. Harrison, and M. Y. M. Chiang, Rev. Sci. Instrum. **76** (6), 062207 (2005).
29. C. M. Stafford, C. Harrison, K. L. Beers, A. Karim, E. J. Amis, M. R. Vanlandingham, H.-C. Kim, W. Volksen, R. D. Miller, E. E. Simonyi, Nat. Mater. **3** (8), 545 (2004).
30. C. M. Stafford, B. D. Vogt, C. Harrison, D. Julthongpiput, R. Huang, Macromolecules **39** (15), 5095 (2006).
31. R. Huang, C. M. Stafford, and B. D. Vogt, J. Aerosp. Eng. **20** (1), 38 (2007).
32. N. Bowden, S. Brittain, A. G. Evans, J. W. Hutchinson, G. M. Whitesides, Nature **393**, 146 (1998).
33. A. L. Volynskii, S. Bazhenov, O. V. Lebedeva, and N. F. Bakeev, J. Mater. Sci. **35**, 547 (2000).
34. J. L. Keddie, R. A. L. Jones, and R. A. Cory, Europhys. Lett. **27**, 59 (1994).
35. A. D. Schwab, D. M. G. Agra, J.-H. Kim, S. Kumar, A. Dhinojwala, Macromolecules **33**, 4903 (2000).
36. J. A. Forrest, C. Svanberg, K. Revesz, M. Rodahl, L. M. Torell, B. Kasemo, Phys. Rev. E: Stat., Nonlinear, Soft Matter Phys. **58**, 1226 (1998).
37. P. Scheidler, W. Kob, and K. Binder, Europhys. Lett. **59**, 701 (2002).
38. P. Scheidler, W. Kob, and K. Binder, J. Phys. Chem. B **108**, 6673.
39. G. D. Smith, D. Bedrov, and O. Borodin, Phys. Rev. Lett. **90**, 226103 (2003).
40. C. E. Porter and F. D. Blum, Macromolecules **33**, 7016 (2000).
41. R. M. Overney, C. Buenviaje, R. Luginbuhl, and F. Dinelli, J. Therm. Anal. Calorim **59**, 205 (2000).
42. C. Bollinne, V. W. Stone, V. Carlier, and A. M. Jonas, Macromolecules **32**, 4719 (1999).
43. B. Frank, A. P. Gast, T. R. Russel, H. R. Brown, C. Hawker, Macromolecules **29**, 6531 (1996).
44. X. Zheng, B. B. Sauer, J. G. V. Alsten, S. A. Schwartz, M. H. Rafailovich, J. Sokolov, M. Rubinstein, Phys. Rev. Lett. **74**, 407 (1995).
45. D. J. Pochan, E. K. Lin, S. K. Satija, and W.-L. Wu, Macromolecules **34**, 3041 (2001).
46. J. Wang, M. Tolan, O. H. Seeck, S. K. Sinha, O. Bahr, M. H. Rafailovich, J. Sokolov, Phys. Rev. Lett. **83**, 564 (1999).
47. A. Van der Lee, L. Hamon, Y. Holl, and Y. Grohens, Langmuir **17** (24), 7664 (2001).
48. L. Hartmann, W. Gorbatschow, J. Hauwede, and F. Kremer, Eur. Phys. J. E: Soft Matter Biol. Phys. **8**, 145 (2002).
49. Y. Mi, G. Xue, and X. Lu, Macromolecules **36** (20), 7560 (2003).
50. Y. Mi, G. Xue, and X. Wang, Polymer **43** (25), 6701 (2002).
51. X. Lu, G. Xue, and Y. Mi, J. Appl. Polym. Sci. **119** (4), 2310 (2011).
52. L. Li, B. Li, J. Chen, D. Zhou, G. Xue, X. Liu, Polymer **45** (8), 2813 (2004).
53. S. C. Pilcher and W. T. Ford, Macromolecules **31** (11), 3454 (1998).
54. Y. Wang, C.-M. Chan, K.-M. Ng, and L. Li, Macromolecules **41** (7), 2548 (2008).
55. H. Yin, S. Napolitano, and A. Schönhals, Macromolecules **45** (3), 1652 (2012).
56. G. B. DeMaggio, W. E. Frieze, D. W. Gidley, M. Zhu, H. A. Hristov, A. F. Yee, Phys. Rev. Lett. **78** (8), 1524 (1997).
57. J. L. Keddie, R. A. L. Jones, and R. A. Cory, Faraday Discuss. **98**, 219 (1994).
58. J. H. van Zanten, W. E. Wallace, and W.-L. Wu, Phys. Rev. E: Stat., Nonlinear, Soft Matter Phys. **53** (3), R2053 (1996).

59. Y. Grohens, M. Brogly, C. Labbe, M.-O. David, J. Schultz, Langmuir **14** (11), 2929 (1998).
60. H. L. Frisch and J. E. Mark, Chem. Mater. **8** (8), 1735 (1996).
61. H. L. Frisch, S. Maaref, Y. Xue, G. Beaucage, Z. Pu, J. E. Mark, J. Polym. Sci., Part A: Polym. Chem. **34** (4), 673 (1996).
62. H. Rudolph, J. Mahrholz, and K. Buchholz, Langmuir **12** (13), 3101 (1996).
63. C. Zhang, Y. Guo, and R. D. Priestle, J. Polym. Sci., Polym. Phys. Ed. **51**, 574 (2013).
64. A. Sharples, *Introduction to Polymer Crystallization* (Edwaed Arnold LTD, London, 1966).
65. Yu. K. Godovskii, *Crystallization of Polymers in Encyclopedia of Polymers* (Sovetskaya entsiklopediya, Moscow, 1972), Vol. 1 [in Russian].
66. L. Mandelkern, *Crystallization of Polymers* (McGraw-Hill, New York, 1964).
67. P. H. Geil *Polymer Single Crystlas* (Interscience Publ., New York, 1964).
68. G. M. Bartenev and S. Ya. Frenkel', *Physics of Polymers* (Khimiya, Leningrad, 1990) [in Russian].
69. Y.-X. Liu and E.-Q. Chen, Coord. Chem. Rev. **254** (9–10), 1011 (2010).
70. H. Wu, W. Wang, Y. Huang, and Z. Su, Macromol. Rapid Commun. **30**, 194 (2009).
71. D. N. Theodorou, Macromolecules **22** (12), 4578 (1989).
72. K. F. Mansfield and D. N. Theodorou, Macromolecules **23** (20), 4430 (1990).
73. K. F. Mansfield and D. N. Theodorou, Macromolecules **24** (15), 4295 (1991).
74. V. A. Harmandaris, K. C. Daoulas, and V. G. Mavrantzas, Macromolecules **38** (13), 5796 (2005).
75. Y. Jiang, D.-D. Yan, X. Gao, C. C. Han, X.-G. Jin, L. Li, Y. Wang, C.-M. Chan, Macromolecules **36** (10), 3652 (2003).
76. Y.-G. Lei, C.-M. Chan, Y. Wang, K.-M. Ng, Y. Jiang, L. Lin, Polymer **44** (16), 4673 (2003).
77. Y.-G. Lei, C.-M. Chan, J.-X. Li, K.-M. Ng, Y. Wang, Y. Jiang, L. Li, Macromolecules **35** (18), 6751 (2002).
78. L. Li, C.-M. Chan, K. L. Yeung, J.-X. Li, K.-M. Ng, Y. Lei, Macromolecules **34** (2), 316 (2001).
79. L. Li, C.-M. Chan, J.-X. Li, K.-M. Ng, K.-L. Yeung, L.-T. Weng, Macromolecules **32** (24), 8240 (1999).
80. Y. Wang, C.-M. Chan, K.-M. Ng, Y. Jiang, L. Li, Langmuir **20** (19), 8220 (2004).
81. D. C. Bassett, Philos. Trans. R. Soc. London **348**, 29 (1994).
82. H. D. Keith and F. J. Padden, J. Appl. Phys. **34** (8), 2409 (1963).
83. H. Schönherr and C. W. Frank, Macromolecules **36** (4), 1188 (2003).
84. Y. Ma, Hu, and G. Reiter, Macromolecules **39** (15), 5159 (2006).
85. C. J. Ellison and J. M. Torkelson, Nat. Mater. **2**, 695 (2003).
86. H. Li and S. Yan, Macromolecules **44** (3), 417 (2011).
87. J. L. Thomason and A. A. Van Rooyen, J. Mater. Sci. **27** (4), 889 (1992).
88. H. Ishida and P. Bussi, Macromolecules **24** (12), 3569 (1991).
89. K. Cho, D. Kim, and S. Yoon, Macromolecules **36** (20), 7652 (2003).
90. J. L. Thomason and A. A. van Rooyen, *The Transcrystallised Interphase in Thermoplastic Composites in Controlled Interphases in Composite Materials*, Ed. by H. Ishida (Springer Netherlands, Dordrecht, 1990).
91. B. Hsiao and E. H. Chen, *Transcrystalline Interphase in Advanced Polymer Composites in Controlled Interphases in Composite Materials*, Ed. by H. Ishida (Springer Netherlands, Dordrecht, 1990).
92. J. J. Varga, J. Mater. Sci. **27**, 2557 (1992).
93. J. Varga and J. Karger-Kocsis, J. Polym. Sci., Polym. Phys. Ed. **34** (4), 657 (1996).
94. J. Varga, Y. Fujiwara, and A. Ille, Period. Polytech., Chem. Eng **34**, 255 (1990).
95. J. Varga, *Crystallization, Melting and Supermolecular Structure of Isotactic Polypropylene in Poly(Propylene): Structure, Blends and Composites*, Ed. by J. Karger-Kocsis (Chapman & Hall, London, 1995), Vol. 1.
96. J. Varga, J. Therm. Anal. **31**, 165 (1986).
97. X. Sun, H. Li, J. Wang, and S. Yan, Macromolecules **39** (25), 8720 (2006).
98. S. Y. Hobbs, Nat. Phys. Sci. **234**, 12 (1971).
99. H. Li, X. Zhang, X. Kuang, J. Wang, D. Wang, L. Li, S. Yan, Macromolecules **37** (8), 2847 (2004).
100. H. Li, X. Sun, S. Yan, and J. M. Schultz, Macromolecules **41** (13), 5062 (2008).
101. H. Li, S. Jiang, J. Wang, D. Wang, S. Yan, Macromolecules **36** (8), 2802 (2003).
102. X. Sun, H. Li, X. Zhang, J. Wang, D. Wang, S. Yan, Macromolecules **39** (3), 1087 (2006).
103. X. Sun, H. Li, X. Zhang, D. Wang, J. M. Schultz, S. Yan, Macromolecules **43** (1), 561 (2010).
104. R. Andrews, D. Jacques, A. M. Rao, T. Rantell, F. Derbyshire, Y. Chen, J. Chen, R. C. Haddon, Appl. Phys. Lett. **75** (9), 1329 (1999).
105. B. Li and C. Y. Li, J. Am. Chem. Soc. **129** (1), 12 (2007).
106. O. Lourie, D. M. Cox, and H. D. Wagner, Phys. Rev. Lett. **81** (8), 1638 (1998).
107. O. Regev, P. N. B. ElKati, J. Loos, and C. E. Koning, Adv. Mater. **16** (3), 248 (2004).
108. A. Koganemaru, Y. Bin, Y. Agari, and M. Matsuo, Adv. Funct. Mater. **14** (9), 842 (2004).
109. E. T. Thostenson, Z. Ren, and T.-W. Chou, Compos. Sci. Technol. **61** (13), 1899 (2001).
110. H. E. Miltner, N. Grossiord, K. Lu, J. Loos, C. E. Koning, B. Van Mele, Macromolecules **41** (15), 5753 (2008).
111. B. P. Grady, F. Pompeo, R. L. Shambaugh, and D. E. Resasco, J. Phys. Chem. B **106** (23), 5852 (2002).
112. L. Li, B. Li, M. A. Hood, and C. Y. Li, Polymer **50** (4), 953 (2009).
113. C. Y. Li, L. Li, W. Cai, S. L. Kodjie, K. K. Tenneti, Adv. Mater. **17** (9), 1198 (2005).

114. L. Li, C. Y. Li, and C. Ni, J. Am. Chem. Soc. **128** (5), 1692 (2006).
115. L. Li, C. Y. Li, C. Ni, L. Rong, B. Hsiao, Polymer **48** (12), 3452 (2007).
116. J. Yue, Q. Xu, Z. Zhang, and Z. Chen, Macromolecules **40** (25), 8821 (2007).
117. Z. Zhang, Q. Xu, Z. Chen, and J. Yue, Macromolecules **41** (8), 2868 (2008).
118. F. Zhang, H. Zhang, Z. Zhang, Z. Chen, Q. Xu, Macromolecules **41** (12), 4519 (2008).
119. X. Zheng and Q. Xu, J. Phys. Chem. B **114** (29), 9435 (2010).
120. L. He, X. Zheng, and Q. Xu, J. Phys. Chem. B **114** (16), 5257 (2010).
121. R. H. Somani, L. Yang, L. Zhu, and B. S. Hsiao, Polymer **46** (20), 8587 (2005).
122. L. Yang, R. H. Somani, I. Sics, B. S. Hsiao, R. Kolb, H. Fruitwala, C. Ong, Macromolecules **37** (13), 4845 (2004).
123. B. S. Hsiao, L. Yang, R. H. Somani, C. A. Avila-Orta, L. Zhu, Phys. Rev. Lett. **94** (11), 117802 (2005).
124. W. Hu, D. Frenkel, and V. B. F. Mathot, Macromolecules **35** (19), 7172 (2002).
125. R. Y. F. Liu, T. E. Bernal-Lara, A. Hiltner, and E. Baer, Macromolecules **37** (18), 6972 (2004).
126. J. M. Carr, D. S. Langhe, M. T. Ponting, A. Hiltner, E. Baer, J. Mater. Res. **27** (10), 1326 (2012).
127. R. Y. F. Liu, Y. Jin, A. Hiltner, and E. Baer, Macromol. Rapid Commun. **24**, 943 (2003).
128. H. Wang, J. K. Keum, A. Hiltner, E. Baer, B. Freeman, A. Rozanski, A. Galeski, Science **323**, 757 (2009).
129. M. Ponting, Y. Lin, J. K. Keum, A. Hiltner, E. Baer, Macromolecules **43** (20), 8619 (2010).
130. H. Wang, J. K. Keum, A. Hiltner, and E. Baer, Macromolecules **43**, 3359 (2010).
131. G. Zhang, P. C. Lee, S. Jenkins, J. Dooley, E. Baer, Polymer **55** (2), 663 (2014).
132. S. S. Ray and M. Okamoto, Prog. Polym. Sci. **28**, 1539 (2003).
133. D. R. Paul and L. M. Robeson, Polymer **49** (15), 3187 (2008).
134. P. B. Messersmith and E. P. Giannelis, Chem. Mater. **6** (10), 1719 (1994).
135. P. B. Messersmith and E. P. Giannelis, J. Polym. Sci., Part A: Polym. Chem. **33** (7), 1047 (1995).
136. A. Usuki, Y. Kojima, M. Kawasumi, A. Okada, Y. Fukushima, T. Kurauchi, O. Kamigaito, J. Mater. Res. **8** (05), 1179 (1993).
137. K. Yano, A. Usuki, A. Okada, T. Kurauchi, O. Kamigaito, J. Polym. Sci., Part A: Polym. Chem. **31** (10), 2493 (1993).
138. S. D. Burnside and E. P. Giannelis, Chem. Mater. **7** (9), 1597 (1995).
139. R. A. Vaia, S. Vasudevan, W. Krawiec, L. G. Scanlon, E. P. Giannelis, Adv. Mater. **7** (2), 154 (1995).
140. P. Aranda and E. Ruiz-Hitzky, Chem. Mater. **4** (6), 1395 (1992).
141. J. Wu and M. M. Lerner, Chem. Mater. **5** (6), 835 (1993).
142. E. P. Giannelis, Adv. Mater. **8** (1), 29 (1996).
143. E. P. Giannelis, R. Krishnamoorti, and E. Manias, Adv. Polym. Sci. **138**, 107 (1999).
144. R. A. Vaia, H. Ishii, and E. P. Giannelis, Chem. Mater. **5** (12), 1694 (1993).
145. R. A. Vaia, PhD Thesis (Cornell Univ., Ithaca, 1995).
146. R. A. Vaia, K. D. Jandt, E. J. Kramer, and E. P. Giannelis, Macromolecules **28** (24), 8080 (1995).
147. S. H. Anastasiadis, K. Karatasos, G. Vlachos, E. Manias, E. Giannelis, Phys. Rev. Lett. **84** (5), 915 (2000).
148. R. A. Vaia, B. B. Sauer, O. K. Tse, and E. P. Giannelis, J. Polym. Sci., Polym. Phys. Ed. **35** (1), 59 (1997).
149. C. L. Jackson and G. B. McKenna, J. Non-Cryst. Solids **131–133** (1), 221 (1991).
150. C. L. Jackson and G. B. McKenna, Chem. Mater. **8** (8), 2128 (1996).
151. J. Zhang, G. Liu, and J. Jonas, J. Phys. Chem. **96** (8), 3478 (1992).
152. F. Kremer, A. Huwe, M. Arndt, P. Behrens, W. Schwieger, J. Phys.: Condens. Matter **11** (A175) (1999).
153. M. Arndt, R. Stannarius, H. Groothues, E. Hempel, F. Kremer, Phys. Rev. Lett. **79** (11), 2077 (1997).
154. K. Chrissopoulou, K. S. Andrikopoulos, S. Fotiadou, S. Bollas, C. Karageorgaki, D. Christofilos, G. A. Voyiatzis, S. H. Anastasiadis, Macromolecules **44**, 9710 (2011).
155. P. Apel, Radiat. Meas. **34** (1–6), 559 (2001).
156. G. P. Crawford, L. M. Steele, R. Ondris-Crawford, G. S. Iannacchione, C. J. Yeager, J. W. Doane, D. Finotello, J. Chem. Phys. **96** (10), 7788 (1992).
157. M. Steinhart, Adv. Polym. Sci. **220**, 123 (2008).
158. R. M. Michell, A. T. Lorenzo, A. J. Müller, M.-C. Lin, H.-L. Chen, I. Blaszczyk-Lezak, J. Martin, C. Mijangos, Macromolecules **45** (3), 1517 (2012).
159. R. M. Michell, I. Blaszczyk-Lezak, C. Mijangos, and A. J. Müller, Polymer **54** (16), 4059 (2013).
160. H. Masuda and K. Fukuda, Science **268**, 1466 (1995).
161. C. R. Martin, Science **266**, 1961 (1994).
162. C. R. Martin, Chem. Mater. **8**, 1739 (1996).
163. J. C. Hulteen and C. R. Martin, J. Mater. Chem. **7**, 1075 (1997).
164. M. Steinhart, R. B. Wehrspohn, U. Gosele, and J. H. Wendorff, Angew. Chem., Int. Ed. **43**, 1334 (2004).
165. M. Steinhart, J. H. Wendorff, A. Greiner, R. B. Wehrspohn, K. Nielsch, J. Schilling, J. Choi, U. Gösele, Science **296**, 1997 (2002).
166. V. M. Cepak and C. R. Martin, Chem. Mater. **11**, 1363 (1999).
167. H. Wu, W. Wang, H. Yang, and Z. Su, Macromolecules **40** (12), 4244 (2007).
168. K. Shin, E. Woo, Y. G. Jeong, C. Kim, J. Huh, K.-W. Kim, Macromolecules **40** (18), 6617 (2007).
169. J. Maiz, J. Martin, and C. Mijangos, Langmuir **28** (33), 12296 (2012).
170. M. Steinhart, S. Senz, R. B. Wehrspohn, U. Gösele, J. H. Wendorff, Macromolecules **36** (10), 3646 (2003).

171. E. Woo, J. Huh, Y. G. Jeong, and K. Shin, Phys. Rev. Lett. **98** (13), 136103 (2007).
172. J. L. Carvalho and K. Dalnoki-Veress, Eur. Phys. J. **34** (6), 1 (2011).
173. K. Lee, G. Yu, E. Woo, S. Hwang, K. Shin, *Freezing and Melting in Nanopores in Adsorption and Phase Behaviour in Nanochannels and Nanotubes*, Ed. by L. J. Dunne and G. Manos (Springer, London; New York, 2009).
174. M. Steinhart, P. Goring, H. Dernaika, M. Prabhukaran, U. Gösele, E. Hempel, T. Thurn-Albrecht, Phys. Rev. Lett. **97**, 027801 (2006).
175. H. Wu, Z. Su, and A. Takahara, Soft Matter **8** (11), 3180 (2012).
176. Z. Hu, G. Baralia, V. Bayot, J.-F. Gohy, A. M. Jonas, Nano Lett. **5** (9), 1738 (2005).
177. J. Martin, C. Mijangos, A. Sanz, T. A. Ezquerra, A. Nogales, Macromolecules **42** (14), 5395 (2009).
178. R. P. Kambour, J. Polym. Sci., Part D: Macromol. Rev. **7**, 1 (1973).
179. E. Passaglia, J. Phys. Chem. Solids **48**, 1075 (1987).
180. A. L. Volynskii and N. F. Bakeev, *Solvent Crazing of Polymers* (Elsevier, Amsterdam; New York, 1996).
181. A. L. Volynskii and N. F. Bakeev, *Structural Self-organization of Amorphous Polymers* (Fizmatlit, Moscow, 2005) [in Russian].
182. A. L. Volynskii, T. E. Grokhovskaya, N. A. Shitov, and N. F. Bakeev, Vysokomol. Soedin., Ser. B **22** (7), 483 (1980).
183. A. L. Volynskii, N. A. Shitov, A. S. Chegolya, and N. F. Bakeev, Vysokomol. Soedin., Ser. B **25** (6), 393 (1983).
184. E. G. Rukhlya, E. A. Litmanovich, A. I. Dolinnyi, L. M. Yarysheva, A. L. Volynskii, N. F. Bakeev, Macromolecules **44**, 5262 (2011).
185. A. L. Volynskii, E. G. Rukhlya, L. M. Yarysheva, and N. F. Bakeev, Dokl. Phys. Chem. **447** (1), 200 (2012).
186. A. Y. Yarysheva, D. B. Bagrov, E. G. Rukhlya, L. M. Yarysheva, A. L. Volynskii, N. F. Bakeev, Polym. Sci., Ser. A **54** (10), 779 (2012).
187. L. M. Yarysheva, B. N. Tarasevich, A. V. Bakirov, A. Y. Yarysheva, E. G. Rukhlya, N. S. Chvalun, A. L. Volynskii, N. F. Bakeev, Dokl. Phys. Chem. **459** (1), 177 (2014).
188. H. Wang, J. K. Keum, A. Hiltner, and E. Baer, Macromol. Rapid Commun. **31** (4), 356 (2010).
189. L. Zhu, S. Z. D. Cheng, B. H. Calhoun, Q. Ge, R. P. Quirk, E. L. Thomas, B. S. Hsiao, F. Yeh, B. Lotz, J. Am. Chem. Soc. **122** (25), 5957 (2000).
190. A. Taden and K. Landfester, Macromolecules **36**, 4037 (2003).
191. D. Zhou, L. Li, Y. Li, J. Zhang, G. Xue, Macromolecules **36** (12), 4609 (2003).
192. G. Xue, Y. Wang, X. Gu, and Y. Lu, Macromolecules **27** (14), 4016 (1994).
193. G. Xue, Y. Wang, S. Liu, and Y. -T. Liao, Macromolecules **28** (12), 4344 (1995).
194. H. Bu, F. Gu, L. Bao, and M. Chen, Macromolecules **31** (20), 7108 (1998).
195. Y. Li and G. Xue, Polymer **40** (11), 3165 (1999).
196. Y. Li and G. Xue, Macromolecules **32** (12), 3984 (1999).
197. Z. Xiao, Q. Sun, G. Xue, Z. Yuan, Q. Dai, Y. Hu, Eur. Polym. J. **39** (5), 927 (2003).
198. Q. Sun, Q. Fu, G. Xue, and W. Chen, Macromol. Rapid Commun. **22** (14), 1182 (2001).
199. L. Chen, Y. Wang, X. Zhu, and D. Yan, Polym. Int. **53** (2), 131 (2004).
200. G. Ji, G. Xue, J. Ma, C. Dong, X. Gu, Polymer **37** (15), 3255 (1996).
201. G. Ji, F. Li, W. Zhu, Q. Dai, G. Xue, X. Gu, J. Macromol. Sci., Pure Appl. Chem. **34** (2), 369 (1997).
202. G. Xue, Y. Wang, S. Liu, and Y. -T. Liao, Macromolecules **28** (9), 3476 (1995).
203. G. Ji, H. Ni, C. Wang, G. Xue, Y. -T. Liao, Macromolecules **29** (7), 2691 (1996).
204. T. Sasaki, N. Yamauchi, S. Irie, and K. Sakurai, J. Polym. Sci., Polym. Phys. Ed. **43** (2), 115 (2005).
205. J. Chen, G. Zheng, L. Xu, Y. Lu, G. Xue, Y. Yang, J. Zhang, Polymer **42** (9), 4459 (2001).
206. M. V. Massa and K. Dalnoki-Veress, Phys. Rev. Lett. **92** (25), 255509 (2004).
207. M. V. Massa, M. S. M. Lee, and K. Dalnoki-Veress, J. Polym. Sci., Polym. Phys. Ed. **43** (23), 3438 (2005).
208. M. V. Massa, J. L. Carvalho, and K. Dalnoki-Veress, Phys. Rev. Lett. **97** (24), 247802 (2006).
209. J. L. Carvalho, M. V. Massa, and K. Dalnoki-Veress, J. Polym. Sci., Polym. Phys. Ed. **44** (24), 3448 (2006).
210. J. L. Carvalho and K. Dalnoki-Veress, Phys. Rev. Lett. **105** (23), 237801 (2010).
211. M. V. Massa, J. L. Carvalho, and K. Dalnoki-Veress, Eur. Phys. J. **12** (1), 111 (2003).
212. D. H. Reneker and I. Chun, Nanotecnology **7** (3), 216 (1996).
213. J. M. Deitzel, J. Kleinmeyer, D. Harris, and N. C. Beck Tan, Polymer **42** (1), 261 (2001).
214. J. H. Yu, S. V. Fridrikh, and G. C. Rutledge, Adv. Mater. **16** (17), 1562 (2004).
215. D. Li and Y. Xia, Adv. Mater. **16** (14), 1151 (2004).
216. D. H. Reneker and A. L. Yarin, Polymer **49** (10), 2387 (2008).
217. A. L. Yarin, Polym. Adv. Technol. **22** (3), 310 (2011).
218. Z.-M. Huang, Y. Z. Zhang, M. Kotaki, and S. Ramakrishna, Compos. Sci. Technol. **63** (15), 2223 (2003).
219. A. Greiner and J. H. Wendorff, Angew. Chem., Int. Ed. Engl. **46** (30), 5670 (2007).
220. J. J. Feng, Phys. Fluids **14** (11), 3912 (2002).
221. J.-H. He and H.-M. Liu, Nonlinear Anal. **63** (2005).
222. E. Zhmayev, D. Cho, and Y. L. Joo, Polymer **51** (1), 274 (2010).
223. Y. Jin, A. Hiltner, and E. Baer, J. Polym. Sci., Polym. Phys. Ed. **45** (10), 1138 (2007).
224. R. Chen and D. Huang, Front. Chem. Eng. China **6** (4), 332 (2011).
225. K. Landfester, Adv. Mater. **13**, 765 (2001).
226. M. Antonietti and K. Landfester, Prog. Polym. Sci. **27**, 689 (2002).

227. F. Price, *Nucleation in Polymer Crystallization in Nucleation*, Ed. by A. C. Zettlemoyer (Marcel Dekker, New York, 1969).
228. B. Vonnegut, J. Colloid Sci. **3**, 563 (1948).
229. D. Turnbull and R. E. Cech, J. Appl. Phys. **21** (8), 804 (1950).
230. G. Pound and V. La Mer, J. Am. Chem. Soc. **74** (9), 2323 (1952).
231. D. Turnbull, J. Chem. Phys. **20** (3), 411 (1952).
232. D. Turnbull and R. Cormia, J. Chem. Phys. **34** (3), 820 (1961).
233. R. L. Cormia, F. P. Price, and D. Turnbull, J. Chem. Phys. **37**, 1333 (1962).
234. J. R. Burns and D. Turnbull, J. Appl. Phys. **37**, 4021 (1966).
235. J. Koutsky, A. Walton, and E. Baer, J. Appl. Phys. **38** (4), 1832 (1967).
236. F. Gornick, G. S. Ross, and L. J. Frolen, J. Polym. Sci., Part C: Polym. Symp. **18** (1), 79 (1967).
237. R. Montenegro, M. Antonietti, Y. Mastai, and K. Landfester, J. Chem. Phys. (in press).
238. *Polymer Blends*, Ed. by C. B. Bucknall and D. R. Paul (Wiley, Weinheim, 2000).
239. M. L. Arnal, M. E. Matos, R. A. Morales, O. O. Santana, A. J. Müller, Macromol. Chem. Phys. **199** (10), 2275 (1998).
240. H. Frensch, P. Harnischfeger, and B. J. Jungnickel, *Fractionated Crystallization in Incompatible Polymer Blends in Multiphase Polymers: Blends and Ionomers*, Ed. by L. A. Utracki and R. A. Weiss (Am. Chem. Soc., Canada, 1989), Vol. 395.
241. G. Zhong, K. Wang, L. Zhang, Z. -M. Li, H. Fong, L. Zhu, Polymer **52** (24), 5397 (2011).
242. H. Luo, Y. Huang, D. Wang, and J. Shi, J. Polym. Sci., Polym. Phys. Ed. **51** (5), 376 (2013).
243. Y. He, B. Zhu, W. Kai, and Y. Inoue, Macromolecules **37** (9), 3337 (2004).
244. D. S. Langhe, J. K. Keum, A. Hiltner, and E. Baer, J. Polym. Sci., Polym. Phys. Ed. **49** (2), 159 (2011).
245. R. V. Castillo, M. L. Arnal, A. J. Müller, I. W. Hamley, V. Castelletto, H. Schmalz, V. Abetz, Macromolecules **41** (3), 879 (2008).
246. H.-L. Chen, J.-C. Wu, T.-L. Lin, and J. S. Lin, Macromolecules **34** (20), 6936 (2001).
247. A. Röttele, T. Thurn-Albrecht, J.-U. Sommer, and G. Reiter, Macromolecules **36** (4), 1257 (2003).
248. Y.-Y. Huang, H.-L. Chen, H.-C. Li, T.-L. Lin, J. S. Lin, Macromolecules **36** (2), 282 (2002).
249. Y.-Y. Huang, C. H. Yang, H.-L. Chen, F.-C. Chiu, T.-L. Lin, W. Liou, Macromolecules **37** (2), 486–493 (2004).
250. A. J. Müller, V. Balsamo, and M. L. Arnal, Adv. Polym. Sci. **190**, 1 (2005).
251. A. J. Müller, V. Balsamo, M. L. Arnal, T. Jakob, H. Schmalz, V. Abetz, Macromolecules **35** (8), 3048 (2002).
252. D. J. Quiram, R. A. Register, G. R. Marchand, and D. H. Adamson, Macromolecules **31** (15), 4891 (1998).
253. R. M. Michell, A. J. Müller, G. Deshayes, and P. Dubois, Eur. Polym. J. **46** (6), 1334 (2010).
254. Z. Li, R. Liu, B. Mai, W. Wang, Q. Wu, G. Liang, H. Gao, F. Zhu, Polymer **54** (6), 1663 (2013).
255. L. Yin and M. A. Hillmyer, Macromolecules **44** (8), 3021 (2011).
256. Y. Suzuki, H. Duran, M. Steinhart, H.-J. Butt, G. Floudas, Macromolecules **47** (5), 1793 (2014).
257. G. Floudas, G. Reiter, O. Lambert, and P. Dumas, Macromolecules **31** (21), 7279 (1998).
258. G. Floudas, G. Reiter, O. Lambert, P. Dumas, F. J. Yeh, B. Chu, *Block Crystallization in Model Triarm Star Block Copolymers with Two Crystallizable Blocks: A Time-Resolved SAXS-WAXD Study in Scattering from Polymers* (Am. Chem. Soc, New York, 1999).
259. S. Jiang, C. He, Y. Men, X. Chen, L. An, S. S. Funari, C.-M. Chan, Eur. Phys. J. E **27**, 357 (2008).
260. U. W. Gedde, *Polymer Physics* (Chapman & Hall, London; New York, 1995).
261. J. L. Tell and H. J. Maris, Phys. Rev. B: Solid State **28**, 5122 (1983).
262. S. Sawamura, H. Miyaji, K. Izumi, S. J. Sutton, Y. Miyamoto, J. Phys. Soc. Jpn. **67** (10), 3338 (1998).
263. K. Dalnoki-Veress, J. A. Forrest, M. V. Massa, A. Pratt, A. Williams, J. Polym. Sci., Polym. Phys. Ed. **39** (21), 2615 (2001).
264. S. Ok and A. L. Demirel, J. Macromol. Sci., Part B: Phys. **42** (3–4), 611 (2003).
265. H. Schönherr and C. W. Frank, Macromolecules **36** (4), 1199 (2003).
266. *Physics of Polymer Surfaces and Interfaces*, Ed. by I. C. Sanchez (Butterworth-Heinemann, Boston, 1992).
267. C. W. Frank, V. Rao, M. M. Despotopoulou, R. F. W. Pease, W. D. Hinsberg, R. D. Miller, J. F. Rabolt, Science **273**, 912 (1996).
268. M. M. Despotopoulou, C. W. Frank, R. D. Miller, and J. F. Rabolt, Macromolecules **28** (19), 6687 (1995).
269. M. M. Despotopoulou, C. W. Frank, R. D. Miller, and J. F. Rabolt, Macromolecules **29** (18), 5797 (1996).
270. J. H. Kim, J. Jang, and W. Zin, Macromol. Rapid Commun. **22**, 386 (2001).
271. Y. Wang, S. Ge, M. Rafailovich, J. Sokolov, Y. Zou, H. Ade, J. Luening, A. Lustiger, G. Maron, Macromolecules **37**, 3319 (2004).
272. H. Schonherr, L. E. Bailey, and C. W. Frank, Langmuir **18**, 490 (2002).
273. G. Reiter, J. Polym. Sci., Polym. Phys. Ed. **41** (16), 1869 (2003).
274. J. S. Langer, Rev. Mod. Phys. **52**, 1 (1980).
275. S. Napolitano and M. Wübbenhorst, Macromolecules **39** (18), 5967 (2006).
276. M. Imai, K. Kaji, T. Kanaya, and Y. Sakai, Phys. Rev. B **52** (17), 12696 (1995).
277. T. A. Ezquerra, E. López-Cabarcos, B. S. Hsiao, and F. J. Baltà-Calleja, Phys. Rev. E: Stat., Nonlinear, Soft Matter Phys. **54** (1), 989 (1996).
278. P. D. Olmsted, W. C. K. Poon, T. C. B. McLeish, N. J. Terrill, A. J. Ryan, Phys. Rev. Lett. **81** (2), 373 (1998).

279. Y.-L. Loo, R. A. Register, and A. J. Ryan, Phys. Rev. Lett. **84** (18), 4120 (2000).

280. L. P. Chang and H. Morawetz, Macromolecules **20** (2), 428 (1987).

281. P. -D. Hong and J.-H. Chen, Polymer **39** (23), 5809 (1998).

282. J. Ding, G. Xue, Q. Dai, and R. Cheng, Polymer **34** (15), 3325 (1993).

283. G. Xue, Y. Lu, G. Shi, and Q. Dai, Polymer **35** (4), 892 (1994).

284. P. Bernazzani, S. L. Simon, D. J. Plazek, and K. L. Ngai, Eur. Phys. J. E **8** (2), 201 (2002).

285. S. L. Simon, P. Bernazzani, and G. B. McKenna, Polymer **44** (26), 8025 (2003).

286. W. Zheng and S. L. Simon, Polymer **47** (10), 3520 (2006).

Translated by T. Soboleva